A STUDY OF THE DYNAMICS OF THE INTERACTION OF CH_4 WITH THE (111) SURFACE OF Rh AND THE (110) SURFACE OF Ir

Thesis by

Jennifer Joanne Zinck

In Partial Fulfillment of the Requirements

for the Degree of

Doctor of Philosophy

California Institute of Technology

Pasadena, California

1985

(Submitted May 31, 1985)

To my brother, Bill.

Acknowledgments

I wish to thank the National Research Council of Canada for supporting me in my first four years of graduate school. The skills of Ray Reed, Seichi Nakawatase, Floyd Litreal, John Yehle, Anton Stark and Kathy Lewis have been invaluable to me.

I must thank my family and friends for the support they have given me over these rather difficult years. In particular, I wish to thank Carol Oken, Buddie Mullins, Eric Hood, Malina Hills and John Vajo for their friendship, encouragement and advice, both professional and personal.

I owe my greatest debt to my husband, Andy, for sharing his ideas with me and for helping me realize that naive questions are, at worst, educational. And to my advisor, Henry Weinberg, thanks so much for the good press!

Abstract

A study of the dynamics associated with the activated dissociative adsorption of CH_4 on the (111) surface of Rh and the (110) surface of Ir has been performed in ultrahigh vacuum (UHV), using laser excitation and molecular beam techniques.

Chapter 2 describes an experiment in which gas phase CH_4 is laser excited to the ν_3 excited vibrational state (8.63 kcal/mole) in a collisionless environment, and also, collisionally deactivated to the $2\nu_4$ state (7.46 kcal/mole), in a He atmosphere. Hydrogen thermal desorption spectra from a Rh(111) surface exposed to the excited gas indicate that, within the experimental limits of detection, no enhancement of dissociative adsorption of CH_4 is obtained by excitation to the ν_3, $2\nu_4$ (or ν_4) vibrational states.

Chapter 3 consists of the description of an ultrahigh vacuum-molecular beam apparatus constructed for the study of gas-surface dynamics. The ultrahigh vacuum chamber is a three level system of custom design. Level I is a load lock for introducing and retrieving the sample, to and from the UHV chamber. The molecular beam axis crosses the UHV chamber at Level II, and also crosses the axis of the ionizer of a quadrupole mass spectrometer detector. Low-energy electron diffraction optics are also mounted at Level II. Auger electron spectroscopy may be performed at Level III. An extended travel UHV sample manipulator has been designed and constructed, which allows translation of the sample to all three levels of the UHV system. The molecular beam line is of a nozzle source design, with three separate chambers which are pumped differentially. A chopper motor, for incident beam modulation, is mounted in the third beam chamber directly adjacent to the UHV chamber, and allows time-of-flight measurements.

Chapter 4 describes an experiment in which the role of translational energy in the chemisorption of CH_4 on Ir(110) is studied via the use of molecular beams of CH_4 seeded in H_2 and He. A probability of dissociative adsorption below 10^{-4} is associated with a CH_4 beam which has an average translational energy of approximately 10 kcal/mole.

The results of Chapters 2 and 4 point to the existence of a barrier to dissociative adsorption of CH_4 that is greater than 10 kcal/mole of total energy, on the surfaces studied. A combination of vibrational and translational activation of CH_4 may be required for dissociative adsorption on Rh(111) and Ir(110).

Table of Contents

CHAPTER 1

INTRODUCTION

Introduction

I. WHAT IS A DYNAMICAL STUDY?

Consider the case of a hypothetical chemical reaction of the atom A with the molecule BC to produce the product molecule AB and the atom C. Assume that the reaction is thermoneutral, and that reactants and products are separated by an energy barrier E_a. If A and BC were rigid spheres, then it would be reasonable to suggest that the reaction

$$A + BC \rightarrow AB + C \tag{1}$$

depends only on the relative velocity of A (BC) with respect to BC (A). However, the diatomic molecule BC has internal degrees of freedom that may participate in a reaction pathway which successfully traverses the barrier to products AB and C. A study which attempts to address every degree of freedom, of all participants in a chemical reaction, is a rigorous dynamical study. In practice, an exact description of a chemical reaction is difficult to obtain, either experimentally or theoretically. However, efforts to address certain aspects of a chemical reaction have produced much useful information, both experimental **(1)** and theoretical **(2)**.

A brief description of some concepts in chemical dynamics and their application to gas-surface interactions is given in this chapter. A sampling of important work is included, but it is by no means a complete survey of the relevant literature. This chapter serves to introduce the ideas and questions pursued in Chapters 2, 3, and 4.

II. CONCEPTS IN DYNAMICS

The classical trajectory calculations of Polanyi **(3)** indicate that identification of which degrees of freedom participate in a chemical reaction provides information concerning the potential energy surface of the reaction. In the case of reaction (1) above, if the crest of the barrier to reaction is in the reactant valley of the potential energy surface, then translational energy in the reactants, versus vibrational energy in the reactants, will be more effective in surmounting it. Conversely, if the crest of the barrier to reaction is in the product valley of the potential energy surface, then reactant vibrational energy, providing that it has the appropriate phase, will be more effective than translational energy in producing reaction to products. It is intuitively appealing, but not correct, to identify the reaction coordinate in these trajectory calculations with the internuclear distance of the species involved in the formation or dissociation of a bond in the chemical reaction. The reaction coordinate is some superposition of all the degrees of freedom available in a system undergoing a reaction, and as a result, a combination of translational, vibrational and rotational modes may be necessary for reaction to occur. (Electronic degrees of freedom are excluded in the present discussion.)

III. WHAT'S INVOLVED IN A STUDY OF GAS-SURFACE DYNAMICS?

A. Ultrahigh vacuum and nozzle source molecular beam techniques.

A great deal of progress in technology has been achieved in the area of ultrahigh vacuum **(4)** and nozzle source molecular beam techniques, in the past 35 years **(5)**. This progress in technology has made the study of the dynamics of gas-surface interactions somewhat less formidable.

1. **The necessity of ultrahigh vacuum (UHV) for surface studies of Group VIII transition metals.**

In order to characterize the interaction of a gas with a solid surface, it is necessary to provide an environment where the interface may be prepared reproducibly, i.e., a vacuum environment in which contamination of the surface by ubiquitous background gases is minimized. For example, the adsorption of H_2 and CO, common components of the background gas, is unactivated on Rh(111), **(6,7)** and Ir(110) **(8,9)**, and the probability of adsorption for H_2 and CO on these surfaces is observed to be high. It is usually necessary to maintain vacuum levels on the order of 10^{-10} torr, to avoid appreciable contamination of the surface by background gases during the course of an experiment.

2. **Nozzle source molecular beams.**

In 1951, Kantrowitz and Grey **(10)** described what has become a prototypical nozzle source molecular beam. The mechanism of the source expansion process itself is complicated and not completely understood **(5)**. It has been observed that a high pressure of gas expanding through a small orifice (typical values are a few atmospheres and 50 microns, respectively), results in a collisionless flow of molecules which is characterized by a narrow velocity distribution (values of $\Delta v/v$ of $< 10\%$ are easily obtained), and an angular distribution of beam intensity from the orifice that is more highly peaked than cosine. The collisionless environment of the beam allows the incident beam molecules to be prepared in an internally excited state with the use of lasers, for example.

B. Dynamical studies of molecular beams incident on transition metal surfaces in UHV

While there have been a considerable number of studies concerning the elastic and inelastic nonreactive scattering of molecular beams with solid

surfaces (11,12), there are comparitively few dynamical studies of reactive scattering of molecular beams from surfaces in UHV. In the case of activated dissociative adsorption on transition metal surfaces, only the systems H_2/Cu (13,14), N2/W (15,16) CH_4/Rh (17,18) and CH_4/Ir (19) have been studied.

IV. SUMMARY

This thesis contains the results of an experiment designed to study the role of vibrational energy in the activated dissocative adsorption of CH_4 on Rh(111) via laser excitation. Also presented, is an experiment designed to study the role of translational energy in the activated dissociative adsorption of CH_4 on the reconstructed Ir(110)-(1x2) surface, using seeded molecular beam techniques. For the latter experiment, an ultrahigh vacuum- molecular beam apparatus has been constructed, which will continue to be used for the study of the dynamics of gas-surface interactions.

REFERENCES

1. See for example, R. B. Bernstein, "Chemical Dynamics via Molecular Beam and Laser Techniques", Clarendon Press, Oxford, 1982.

2. See for example, R. A. Marcus, Faraday Disc. of the Chem. Soc. **55**, 9 (1973).

3. J. C. Polanyi, Acc. Chem. Res. 5, 161 (1971).

4. See for example, A. Roth, "Vacuum Technology", North-Holland Publishing Co., NY, 1979.

5. See for example, P. P. Wegener, "Molecular Beams and Low Density Gas-dynamics", Marcel Dekker Inc, NY, 1974.

6. J. T. Yates, Jr., P. A. Thiel and W. H. Weinberg, Surface Sci. **84**, 427 (1979).

7. P. A. Thiel, E. C. Williams, J. T. Yates, Jr. and W. H. Weinberg, Surface Sci. **84**, 54 (1979).

8. D. E. Ibbotson, T. S. Wittrig and W. H. Weinberg, J. Chem. Phys. **72**, 4885 (1980).

9. J. L. Taylor, D. E. Ibbotson and W. H. Weinberg, J. Chem. Phys. **69** 4298 (1978).

10. A. Kantrowitz and J. Grey, Rev. Sci. Instrum. **22**, 333 (1951).

11. G. Benedek and U. Valbusa, "Dynamics of Gas-Surface Interactions", Springer-Verlag, Berlin, 1982.

12. F. O. Goodman and H. Y. Wachman, "Dynamics of Gas-Surface Scattering", Academic Press, NY, 1976.

13. M. Balooch, M. J. Cardillo, D. R. Miller and R. E. Stickney, Surface Sci. **46**, 358 (1978).

14. M. Balooch and R. E. Stickney, Surface Sci. **44**, 310 (1974).

15. D. J. Auerbach, H. E. Pfnur, C. T. Rettner, J. E. Schlaegel, J. Lee and R. J. Madix, J. Chem. Phys. **81**, 2515 (1984).

16. J. Lee, R. J. Madix, J. E. Schlaegel and D. J. Auerbach, Surface Sci. **143**, 626 (1984).

17. C. N. Stewart and G. Ehrlich, J. Chem. Phys. **62**, 4672 (1975).

18. S. G. Brass, D. A. Reed and G. Ehrlich, J. Chem. Phys. **70**, 5244 (1979).

19. J. J. Zinck, C. B. Mullins and W. H. Weinberg, Chapter 4 of this thesis.

CHAPTER 2

SEARCH FOR VIBRATIONAL ACTIVATION IN THE CHEMISORPTION OF METHANE

[The text of Chapter 2 consists of an article coauthored with John T. Yates, Jr., Sally Sheard and W. H. Weinberg which has appeared in *Journal of Chemical Physics* **70**, 2266 (1979).]

Abstract

Direct laser excitation of the excited ν_3 and $2\nu_4$ vibrational modes of CH_4 has been used to determine whether either state is active for inducing CH_4 dissociative chemisorption on the (111) surface of Rh. The *upper limit* of the efficiency of chemisorption from either of these states was measured to be approximately 5×10^{-5}. This experimental finding suggests that thermally activated dissociation of CH_4 on metal surfaces may proceed via hydrogen atom tunneling from higher excited states or via H···H vibrational extensions which are greater than those experienced in the excited ν_3 or $2\nu_4$ vibrational states.

Search for vibrational activation in the chemisorption of methane

J. T. Yates, Jr.,[a] J. J. Zinck,[b] S. Sheard,[c] and W. H. Weinberg[d]

Division of Chemistry and Chemical Engineering, California Institute of Technology, Pasadena, California 91125
(Received 17 October 1978)

Direct laser excitation of the excited ν_3 and $2\nu_4$ vibrational modes of CH_4 has been used to determine whether either state is active for inducing CH_4 dissociative chemisorption on the (111) surface of Rh. The *upper limit* of the efficiency of chemisorption from either of these states was measured to be approximately 5×10^{-5}. This experimental finding suggests that thermally activated dissociation of CH_4 on metal surfaces may proceed via hydrogen atom tunneling from higher excited states or via H···H vibrational extensions which are greater than those experienced in the excited ν_3 or $2\nu_4$ vibrational states.

I. INTRODUCTION

It is well known that the chemisorption of molecules is often associated with bond breaking to form adsorbed fragments. In certain cases, the activation energy is very small (or zero) and dissociative chemisorption occurs at low temperatures. For saturated hydrocarbon molecules, however, activated chemisorptive fragmentation is often observed.[1] There is currently a great deal of interest in understanding the role of vibrational excitation in inducing the activated chemisorption of molecules. By understanding the vibrational motions responsible for promoting chemisorption, one can visualize the nature of the potential energy surface experienced by the molecule as it dissociates and also the nature of the transition complex through which dissociative chemisorption proceeds.

In a recent theoretical treatment, Gelb and Cardillo[2] have performed classical trajectory calculations for the interaction of H_2 with Cu(100) and Cu(110) surfaces. It was found that, for H_2 (having 5 kcal/mole normal translational energy), there was a 40-fold increase in the probability of dissociation on Cu(100) when the H_2 molecule possessed one quantum of vibrational energy. The importance of the excitation of vibrations in promoting homogeneous chemical reactions is also suggested by classical trajectory calculations, such as those of Polanyi and Wong,[3] where it was shown that the energy of vibrational excitation may induce chemical reactivity more effectively than equivalent translational energy for certain types of potential surfaces.

Experimental measurements have confirmed that, in certain cases, one or two quanta of vibrational energy may influence the reaction probability strongly, e.g., $HCl(\nu=1)+K\rightarrow KCl$, 100-fold enhancement[4]; $HCl(\nu=1)+O\rightarrow OH+Cl$, 400-fold enhancement[5]; and $HCl(\nu=2)+Br\rightarrow HBr+Cl$, 10^{11}-fold enhancement.[6] Direct experimental evidence for single quantum vibrational enhancement of reactions at surfaces is almost nonexistent, although there are examples of heterogeneous processes which are enhanced by multiphoton excitation of reactant molecules.[7,8]

In the work reported here, we have used a He/Ne infrared laser to excite either the ν_3 or $2\nu_4$ vibrational modes of $CH_4(g)$ in the vicinity of a Rh(111) surface. Following irradiation, thermal desorption of products from the crystal has been monitored using a quadrupole mass spectrometer to detect surface species originating from the laser-excited CH_4. The thermal desorption technique is very sensitive since it integrates the number of excited molecules which adsorb over the entire time of irradiation. Precision on the order of $\pm1\%$ of a monolayer of hydrogen has been achieved in comparing experiments involving the laser with control exposures without the laser.

This work is based on an earlier study of the activated chemisorption of CH_4 performed by Stewart and Ehrlich.[9] In their work, it was found that a heated molecular beam of CH_4 contained species which led to irreversible chemisorption on a Rh field emission tip, and it was concluded that vibrational excitation of CH_4 (possibly as the ν_4-CH_4 state) was responsible for the effect. Because of the stringent vacuum conditions necessary in experiments of this type, we have employed the vacuum and gas handling procedures devised by Stewart and Ehrlich[9] wherever possible. We have also increased the sensitivity of the measurement far beyond that obtained in the field emission-heated CH_4 beam experiment.

II. SPECTROSCOPY OF CH_4

A. Energy levels and deactivation processes

The excitation and decay of the vibrational modes of CH_4 have been well studied by Moore and co-workers within the last ten years using infrared laser techniques.[10–16] A schematic energy level diagram is shown in Fig. 1 for CH_4 excitation and subsequent deactivation. For CH_4 in a collisionless situation ($P\lesssim10^{-4}$ torr), the infrared laser simply excites CH_4 to the ν_3 level. Decay of ν_3-CH_4 may possibly occur via wall collisions[10,12] or via fluorescence. For CH_4 in a pure He background, vibration–vibration (v–v) transitions may efficiently occur, causing ν_3-CH_4 to convert to $2\nu_4$-CH_4 with a probability of approximately 5.3

---

[a] Sherman Fairchild Distinguished Scholar. Permanent address: National Bureau of Standards, Washington, D.C. 20234.

[b] National Research Council of Canada Predoctoral Fellow.

[c] National Science Foundation Predoctoral Fellow.

[d] Alfred P. Sloan Foundation Fellow, and Camille and Henry Dreyfus Foundation Teacher–Scholar.

 0021-9606/79/052266-07$01.00

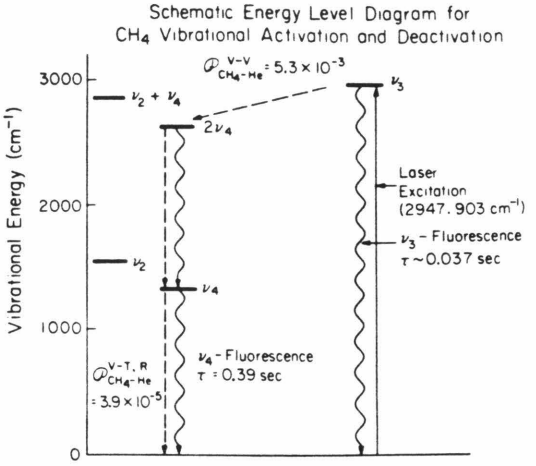

FIG. 1. Schematic energy level diagram for CH_4 vibrational activation and deactivation (taken from Refs. 10–16).

$\times 10^{-3}$ per ν_3-CH_4–He collision.[16] The $2\nu_4$-CH_4 state produced in this manner decays very slowly to ν_4-CH_4, by means of transitions of low collision efficiency of the order of 10^{-5}.[17] The resulting ν_4-CH_4 state is also long lived and decays to the ground state via (v–t or v–r) transitions of low collision efficiency (approximately 3.9×10^{-5}) or by fluorescence.[16] A rapid equilibrium is established between ν_2-CH_4 and ν_4-CH_4 by means of other processes. Thus, by carrying out experiments at low CH_4 pressures, we can produce ν_3-CH_4 as the activated molecule. By operating in a background pressure of pure He, one can efficiently convert the excitation to $2\nu_4$-CH_4.

B. Excitation probability for ν_3-CH_4 and $2\nu_4$-CH_4

The laser used in this work supplies 0.017 W of 2947.903 cm^{-1} (3.39 μ) radiation in a 0.2 cm diameter beam. This laser line overlaps the $P(7)$ CH_4 vibration–rotation line centered at 2947.906 cm^{-1} which is Doppler broadened by 0.009 cm^{-1} at 300 K.[11] The low pressure extinction coefficient for absorption of the laser line has been reported to have the value of 0.12 $cm^{-1}\,torr^{-1}$ by Moore.[11] We have carried out a direct extinction coefficient measurement using a NaCl infrared cell containing CH_4 at various pressures. Transmitted laser power was detected with a Laser Precision RkP-345 radiometer detector (1.5% accuracy) with corrections being made for window losses and impurity radiation at 8680 cm^{-1}. The results are shown in Fig. 2. The measured value of $\epsilon = 0.14$ $cm^{-1}\,torr^{-1}$ is in satisfactory agreement with the earlier result. The rate of ν_3-CH_4 excitation from this laser beam in a 1 cm path length is 3.79×10^{16} molecules $s^{-1}\,torr^{-1}$. With the He background pressure, essentially the same rate of production of $2\nu_4$-CH_4 would be expected.

III. EXPERIMENTAL

A. Vacuum apparatus

The apparatus shown in Fig. 3 was used in these measurements. The apparatus is divided into two major sections by a capillary leak. An ultrahigh vacuum ($\leq 2\times10^{-9}$ torr) gas handling section to the left was pumped with a liquid nitrogen trapped mercury diffusion pump. Spectroscopic grade CH_4 (Linde, analyzed) was transferred at approximately 5 torr to a getter bulb consisting of a freshly evaporated 300 cm^2 Ni film maintained at 195 K. A second getter was employed for further purification of the CH_4 at 195 K. This procedure was used to remove H_2 impurity as well as other reactive impurities from the CH_4.[9]

The purified CH_4 could be quantitatively admitted to the laser cell side of the vacuum system through a capillary leak, the conductance of which is 1.9×10^{13} CH_4 molecules $torr^{-1}\,s^{-1}$, using a bakeable capacitance manometer for measurement of CH_4 pressure behind the capillary leak. The ultrahigh vacuum ($<2\times10^{-10}$ torr) laser cell side of the apparatus ($V = 1.9\times10^3$ cm^3) was constructed almost entirely of quartz and Pyrex to minimize H_2 outgassing from metal surfaces. It consists of an irradiation cell containing quartz windows at the Brewster angle with 12 cm internal path length. The system pumping speed using the ion pump is approximately 2000 $cm^3\,s^{-1}$. A Rh(111) single crystal (0.3 cm^2 front surface area) disk is mounted on Ta heating wires and welded to W/5%Re–W/26%Re thermocouple wires of 0.013 cm diameter. The crystal assembly is held with Ni support leads bolted to 0.63 cm diameter Cu feed throughs which may be cooled externally. Crystal temperatures of 240 K were employed routinely. Static exposures to CH_4 or CH_4 + He were employed in this work by isolating the laser cell from the ion pump using valve V_1.

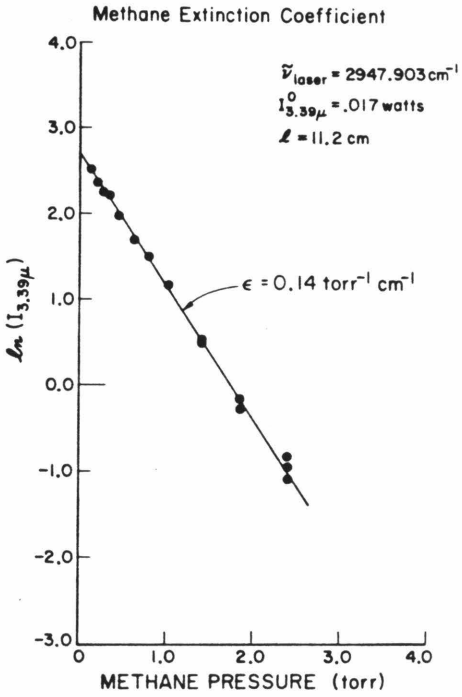

FIG. 2. Methane extinction coefficient.

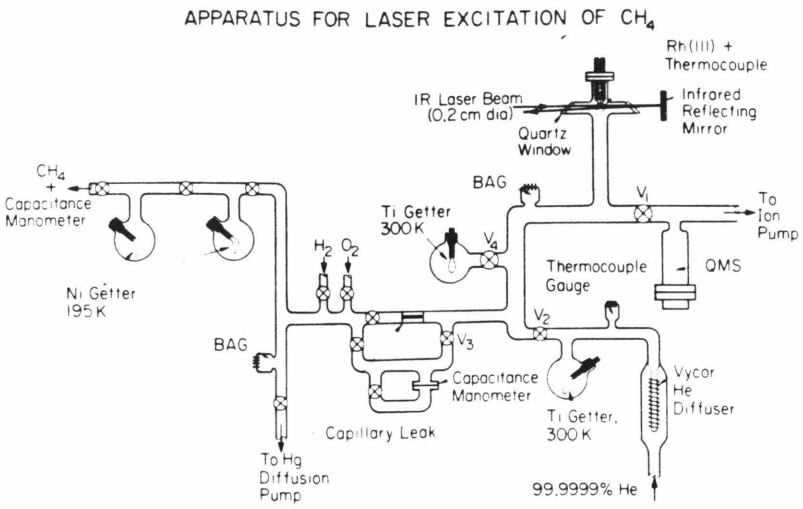

FIG. 3. Ultrahigh vacuum apparatus for laser activation of CH_4 followed by collision with Rh(111).

Under these static conditions, pumping of active residual gases was carried out effectively by opening valve V_4 to a 300 cm^2 freshly deposited Ti getter film (300 K). It was shown that the Ti had no effect on CH_4, in agreement with other work.[18] The Bayard-Alpert gage was not operated during these measurements because of the destructive influence of electron impact and hot filaments on CH_4.[18,19] The laser cell apparatus could be filled with highly purified He through valve V_2. This He was produced by effusion of 99.9999% He through a hot vycor (925 K) thimble, followed by storage over a freshly evaporated Ti getter film. It was shown that the He contains approximately 2×10^{-11} parts H_2/He by separate adsorption experiments on Rh(111).[20]

B. Rh(111) crystal preparation

The preparation and cleaning of Rh(111) has been described previously,[21–23] as has the chemisorption of H_2 by this crystal.[24] The crystal employed in these experiments was cleaned on its front face by Ar^+ bombardment and O_2 treatments in a separate uhv apparatus. Boron impurity was removed permanently from the entire bulk of the crystal using these cleaning procedures, and both Auger spectroscopy and LEED experiments were employed to characterize the clean Rh(111) surface.[21] Following crystal transfer to the laser cell apparatus, the O_2 cleaning procedure was repeated, followed by thermal cleaning at 1260 K. Thermal desorption spectra of H_2 indicated that the behavior of this cleaned crystal in the laser apparatus was identical to that observed for the crystal when its cleanliness had been confirmed with Auger spectroscopy.[24] A sequence of typical H_2 thermal desorption traces is shown in Fig. 4. Separate H_2–D_2 exchange experiments have shown that complete isotopic mixing occurs between hydrogen species in the adsorbed layer, indicating that dissociative adsorption takes place to produce the adsorbed hydrogen layer.[24]

C. Gas handling procedures

It was anticipated that laser excitation of CH_4 would lead to dissociative chemisorption and that this would be subsequently detected by means of H_2 thermal desorption from the Rh(111) crystal. It was therefore important to minimize impurity H_2 adsorption by the crystal during gas handling. This was done by employing the Ti getter pump during static experiments and by preventing ion pump regurgitation of H_2 by means of preliminary pumping of gases from the laser cell following laser irradiation using the mercury diffusion pump through valve V_3. Following pumping into the 10^{-5} torr region, V_3 was closed and the ion pump valve V_1 opened slowly to achieve final background pressure

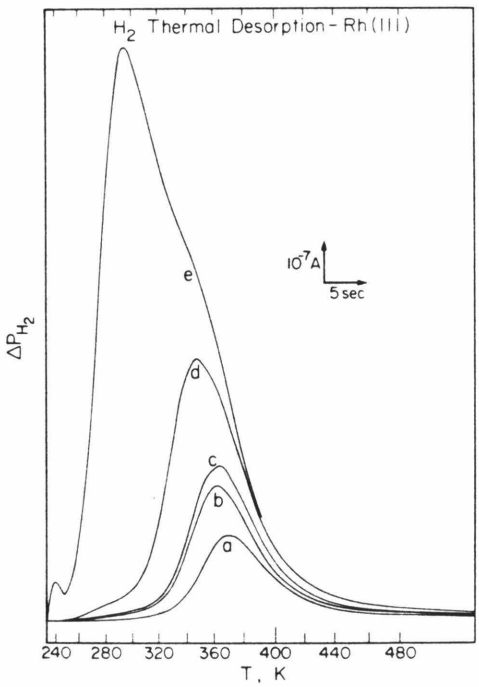

FIG. 4. Hydrogen thermal desorption from Rh(111) for various H_2 exposures up to saturation.

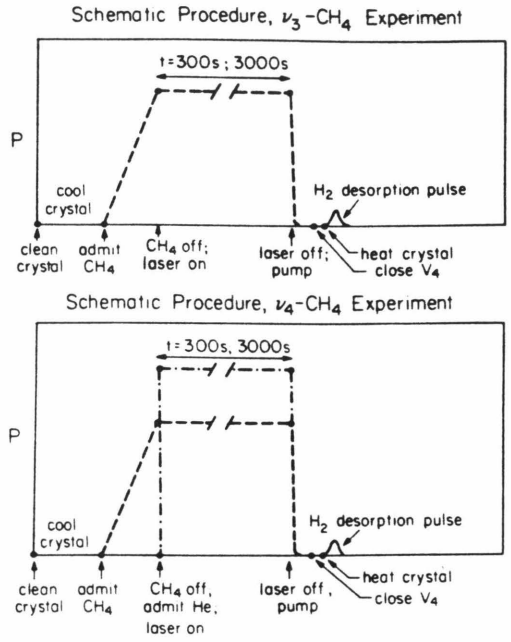

FIG. 5. Schematic procedure for each laser excitation experiment.

suitable for the H_2 thermal desorption measurement. A schematic diagram of the gas handling and laser irradiation schedule is shown in Fig. 5 for both the ν_3-CH_4 and the ν_4-CH_4 experiments.

D. Laser irradiation

A region 0.6 cm in front of the Rh(111) crystal was irradiated with two infrared beams by employing a single reflection beyond the rear Brewster angle window. The losses of infrared energy by absorption and reflection are small. The total path length within the cell for the two beams is 24 cm. However, not all of the excited CH_4 molecules produced along this path will reach the crystal. We assume that one half of the excited molecules from a 2 cm total path length near the front surface of the crystal are incident on the front surface of the crystal. In the case of ν_3-CH_4 excitation, the excited molecules arrive by means of line-of-sight paths from the irradiation region since gas phase collisions are not present. In the case of $2\nu_4$-CH_4, excitation is followed by random walk trajectories due to CH_4–He collisions which lead to $2\nu_4$-CH_4 production. Approximately 200 He/CH_4 collisions are required to achieve ν_3-CH_4 relaxation to $2\nu_4$-CH_4.[16] Therefore, depending on the He pressure, the $2\nu_4$-CH_4 will originate from an expanded cylindrical region surrounding the laser beam. The radius of this cylindrical region of deactivation will decrease as P_{He} is increased. An approximate upper limit of the radius of the activation region r^*_{200} may be estimated in the following manner:

For random walk diffusion of CH_4 through a background pressure of He,

$$r^*_{200} = (2Dt_{200})^{1/2}. \tag{1}$$

The collision rate f for a CH_4 molecule is

$$f = \bar{v}/\lambda, \tag{2}$$

where $\bar{v}$ is the mean velocity and λ is the mean free path. The mutual diffusion coefficient D is

$$D = \tfrac{1}{6} f\lambda^2 = \tfrac{1}{6}\bar{v}\lambda \tag{3}$$

and the mean time required for 200 CH_4–He collisions is

$$t_{200} = 200\lambda/\bar{v}. \tag{4}$$

Therefore,

$$r^*_{200} = \left(\frac{200}{3}\right)^{1/2}\lambda,$$

$$\lambda = \frac{1}{\sqrt{2}}\frac{kT}{\pi P\sigma_{12}^2} = \frac{6.83\times10^{-3}}{P}\,\text{cm}, \tag{5}$$

where P is the pressure in torr, and $\sigma_{12} = 3.2\times10^{-8}$ cm is the mutual collision diameter. Therefore,

$$r^*_{200} = \frac{5.58\times10^{-2}}{P}\,\text{cm}. \tag{6}$$

Therefore, in the He pressure range used in this experiment (0.03–0.60 torr), $0.093 \le r^*_{200} \le 1.86$ cm. This range of r^*_{200} is comparable to the dimensions of the crystal (0.6 cm) and the separation of the crystal from the irradiation region (0.6 cm) so that favorable interception of $2\nu_4$-CH_4 by the crystal should occur. The assumption of the interception of half of the excited $2\nu_4$ molecules produced along a 2 cm path length directly in front of the Rh(111) crystal is reasonable.

E. Detection of chemisorbed hydrogen following laser irradiation

As shown in Fig. 5, thermal desorption mass spectrometry is used to detect hydrogen desorption following laser irradiation of the CH_4 near the front surface of the crystal. Our procedure consists of direct comparison of pairs of experiments in which the quantity of hydrogen adsorbed with the laser on is compared with the quantity adsorbed in control experiments with the laser off. Subtraction of the two integrated desorption spectra is a measure of the effect of the laser. Because of residual hydrogen present in the apparatus or regurgitated by the ion pump when it is open to the laser cell, there is a background hydrogen coverage which is subtracted from the hydrogen coverage detected following laser irradiation. For the experiments performed, the range of the background hydrogen coverage in the control experiments is given in Table I. The quantity of hydrogen (as atoms) on the 0.3 cm^2 crystal is defined to be N_H.

The mass spectrometer was calibrated frequently by measuring the yield of hydrogen from the fully hydrogen-covered Rh(111) surface in control experiments.

IV. EXPERIMENTAL RESULTS

A. ν_3-CH_4

The results for all ν_3-CH_4 experiments are shown in Fig. 6. By employing different CH_4 pressures and ir-

TABLE I. Range of experimental parameters and hydrogen background adsorption in control experiments.

Excited mode	Time of irradiation (s)	Pressure of CH_4 (torr)	Pressure of He (torr)	Fractional hydrogen coverage	Number of adsorbed hydrogen atoms[a] N_H
ν_3-CH_4	300	$7-160\times10^{-6}$	0	0.04–0.09	$1.9-4.3\times10^{13}$
$2\nu_4$-CH_4	300	140×10^{-6}	0.03–0.06	0.04–0.09	$1.9-4.3\times10^{13}$
ν_3-CH_4	3000	$\sim140\times10^{-6}$	0	0.07–0.10	$3.4-4.8\times10^{13}$
$2\nu_4$-CH_4	3000	140×10^{-6}	0.2–0.4	0.07–0.10	$3.4-4.8\times10^{13}$

[a]This number is calculated assuming that saturation coverage of hydrogen is 1.6×10^{15} atoms/cm^2 = 1 atom/Rh on Rh(111). $N_H^{sat} = 4.8\times10^{14}$ atoms on the 0.3 cm^2 surface.

radiation times of 300 or 3000 s, it was possible to extend the range of interception of excited ν_3-CH_4 molecules from 7×10^{13} to 1.5×10^{16} molecules. No trend toward increasing hydrogen yield from the Rh(111) surface is observed in these experiments as exposure to ν_3-CH_4 is increased 200-fold. We may calculate an upper limit $\epsilon^*_{\nu_3}$ for the surface reactivity of ν_3-CH_4 using the average of the pair of points at the extreme right in the figure. Based on the instability of chemisorbed hydrocarbon fragments at temperatures reached in our thermal desorption measurements (580 K), one ν_3-CH_4 molecule will produce 4H(ads) upon decomposition. Therefore,

$$\epsilon^*_{\nu_3} = \frac{\Delta N_H}{4N^*_{\nu_3}} = (5\pm6)\times10^{-5},$$

where ΔN_H is the differential H atom yield due to laser excitation, and $N^*_{\nu_3}$ is the total number of ν_3-CH_4 molecules incident on the crystal.

B. $2\nu_4$-CH_4

The results of all $2\nu_4$-CH_4 experiments are shown in Fig. 7. Two irradiation periods of 300 and 3000 s were employed using He background pressures from 0.03 to 0.60 torr. Again, no significant trend is observed for a tenfold increase in $2\nu_4$-CH_4 production by comparing the 3000 s data to the 300 s data. We may calculate an upper limit $\epsilon^*_{2\nu_4}$ for the reactivity of $2\nu_4$-CH_4 using the average of the 3000 s points. Recognizing that one $2\nu_4$-CH_4 molecule would produce 4H(ads) upon decomposition,

$$\epsilon^*_{2\nu_4} = \frac{\Delta N_H}{4N^*_{2\nu_4}} = (5\pm9)\times10^{-5}.$$

For the 300 s points, we obtain a value of $(8\pm52)\times10^{-5}$ for the upper limit of efficiency for $2\nu_4$-CH_4 decomposition on Rh(111). A search for other products of desorption from the Rh(111) surface was made using the mass spectrometer and observing m/e from 1 to 44. No products other than H_2 and CO were observed to desorb at a sensitivity of 4×10^{-3} of the H_2 desorption yield from a surface saturated with hydrogen.

V. DISCUSSION

A. Comparison with thermal beam experiments

These experiments indicate that the excitation of two CH_4 vibrational modes ν_3 and $2\nu_4$ has at most a very small effect on surface reactivity, causing $\lesssim5\times10^{-5}$ of the *excited* molecules to chemisorb on the Rh(111) surface at 240 K.

It is instructive to compare these results with the thermal excitation measurements of Stewart and Ehrlich.[9] They found that heated CH_4 exhibited an activated adsorption behavior with a 7 kcal/mole barrier (~ 2500 cm^{-1}). In contrast, CD_4 was found to be unreactive at temperatures below 705 K. They attributed this difference in behavior to the slight difference between the H–H rms vibrational amplitude and the D–D rms vibrational amplitude (difference at 705 K ≃ 0.014 Å) in the HCH bending mode. This mode was selected because the distortion of the molecule is greater in this type of vibration than in others (at 705 K, in CH_4, the H–H rms amplitude is 0.13 Å).

It is possible from the field emission data to estimate approximately the coverage of hydrogen or other species

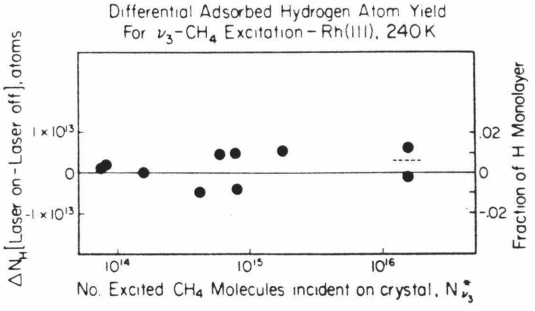

FIG. 6. Differential adsorbed hydrogen atom yield for ν_3-CH_4 excitation. Rh(111) at 240 K.

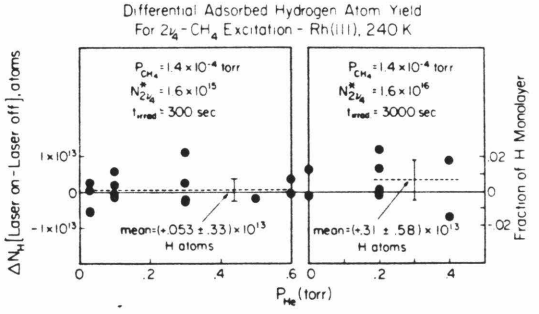

FIG. 7. Differential adsorbed hydrogen atom yield for ν_4-CH_4 excitation. Rh(111) at 240 K.

TABLE II. Fraction of excited CH_4 states at 705 K.

$$\frac{n_i}{N} = \frac{g_i e^{-h\nu_i/kT}}{\pi_i q_i}; \quad q_i = \left(1 - e^{-h\nu_i/kT}\right)^{-g_i}$$

Mode	Frequency (cm^{-1})	Degeneracy g_i	Population ratio n_i/N
ν_1	2914	1	0.0019
ν_2	1526	2	0.0647
ν_3	3020	3	0.0046
ν_4	1306	3	0.152
$2\nu_4$	2600	3	0.0108

detected when the heated CH_4 beam was incident on the Rh field emission tip. Assuming that the measured background effects were on the order of 1% of a monolayer as reported,[9] it would follow that the decrease in field emission current for a CH_4 (705 K) exposure of 0.88×10^{18} molecules cm^{-2} is equivalent to a coverage θ_H on the order of 10% of a monolayer. In Table II, the statistical fraction of the various excited vibrational states of CH_4 in the thermal beam at 705 K is shown; these values are used in the calculation below.

In the field emission experiments, at a CH_4 temperature of 705 K, the highest incident exposure of $2\nu_4$-CH_4, i.e., $N^*_{2\nu_4}$, was therefore 9.2×10^{15} cm^{-2}, while the highest exposure of ν_3-CH_4, i.e., $N^*_{\nu_3}$, was 4×10^{15} cm^{-2}. Since each reactive CH_4 molecule yields 4H(ads), one may calculate the efficiency of reaction $\epsilon^T_{\nu_i}$ for each of the excited vibrational states in the thermal beam, assuming that the saturation coverage of hydrogen on Rh(σ_H^{max}) is 1.6×10^{15} atoms cm^{-2}, *and that each state is alone responsible for the effect.* Thus,

$$\epsilon^T_{2\nu_4} = \frac{\sigma_H^{max}\theta_H}{4N^*_{2\nu_4}} \simeq 4.3\times10^{-3}.$$

Also,

$$\epsilon^T_{\nu_3} \simeq 1\times10^{-2}.$$

Our laser excitation measurements have shown that $\epsilon^*_{2\nu_4}$ is two orders of magnitude smaller than the thermal beam experiment would indicate, or possibly that $\epsilon^*_{2\nu_4}$ is *zero*. On this basis, $\epsilon^*_{\nu_4}$ would also be vanishingly small. Furthermore, the involvement of ν_3-CH_4 as a precursor to chemisorption in the thermal beam experiment is also excluded by our measurements. The ν_3-CH_4 state was excluded on principle by Stewart and Ehrlich[9] on the basis of the small molecular distortion involved in this vibrational mode.

The following *alternative* conclusions may be reached with respect to the result seen by Stewart and Ehrlich[9] compared to the negative result seen in the laser excitation experiment described here:

(1) The activated process involves vibrational states other than ν_3, $2\nu_4$, or ν_4. These could be ν_1, ν_2, a combination mode such as $\nu_2+\nu_4$, or multiquanta vibrational states.

(2) The dissociation of vibrationally excited CH_4 occurs on crystallographic orientations of Rh other than the (111).

(3) Hydrogen impurity was produced in the Pyrex furnace used by Stewart and Ehrlich to heat the CH_4; CD_4 is not so readily decomposed thermally to form D_2 in accordance with the findings of Winters.[18] The impurity hydrogen is responsible for the irreversible chemisorption detected by field emission using heated CH_4 beams, and the lack of an effect with heated CH_4 is due to its stability in the furnace.

B. Comparison with CH_4 chemisorption on tungsten

A second general model for the dissociative adsorption of CH_4 on tungsten (and probably other metals) has been advanced by Winters[18,19] on the basis of studies of the reaction of methane with heated tungsten. In this model, heated CH_4 is allowed to populate various excited vibrational states. Dissociation from the vibrationally excited CH_4 occurs by hydrogen atom quantum mechanical tunneling through a barrier to form CH_3(ads) + H(ads). CH_3(ads) then decomposes rapidly to C(ads) + 3H(ads). A large kinetic isotope effect has been observed with reaction rates decreasing as the extent of deuterium substitution was increased in the five isotopic methane molecules studied.

The model of Winters suggests that the rate of CH_4 decomposition should be related directly to the surface lifetime of the physically adsorbed CH_4^* molecule. Since, in Winters' experiments, surface lifetimes were short, the reaction probability must necessarily be low. In our laser excitation experiments, we are able to produce CH_4 vibrational excitation without heating the metal surface, and hence we are producing relatively long-lived surface–CH_4 species having thousands of times the surface lifetime of the CH_4 used in Winters' lowest temperature experiments on heated tungsten (approximately 600 K), where a reaction probability of 10^{-4} was observed.

Assuming we are exciting CH_4 into the correct vibrational state (ν_3 or $2\nu_4$), and that the state does not lose its vibrational energy to the metal rapidly, one would expect a greatly enhanced reactivity based on the tunneling model. The low reactivity observed for the *excited* ν_3 or $2\nu_4$ species ($\lesssim5\times10^{-5}$) suggests the following:

(1) Insufficient vibrational excitation is available in the excited ν_3- or $2\nu_4$-CH_4 state. Higher excited states must be populated to achieve dissociative adsorption via tunneling.

(2) Another state must be excited to achieve appropriate activation for dissociative chemisorption.

(3) The dynamics of the interaction of CH_4 with tungsten and rhodium are quite different.

VI. CONCLUSIONS

Laser excitation has been used to show that little or no enhancement of CH_4 reactivity with a Rh(111) surface occurs in the ν_3, $2\nu_4$, or ν_4 vibrational states. The *upper limit* for the efficiency of reaction of CH_4 molecules in the ν_3 or $2\nu_4$ state is approximately 5×10^{-5}.

Possible models to produce dissociative adsorption include hydrogen atom tunneling from higher vibrationally excited states, or greater H···H extension than is realized in the excited $2\nu_4$-CH_4 state.

A combination of translational and vibrational energy may be required to produce dissociative chemisorption of CH_4 on Rh.

Sites other than those found on the close packed Rh(111) surface may be required for dissociative chemisorption of CH_4 from an excited vibrational level.

ACKNOWLEDGMENTS

Principal support of this research was derived from the Department of Energy, Division of Basic Energy Sciences. Additional support was obtained from the National Science foundation under Grant No. DMR77-14976.

We thank Professor J. L. Beauchamp for use of the absolute laser power detector. We also thank Professor C. B. Moore for helpful discussions regarding this work.

[1]J. T. Yates, Jr. and T. E. Madey, Surf. Sci. **28**, 437 (1971).
[2]A. Gelb and M. J. Cardillo, Surf. Sci. **64**, 197 (1977).
[3]J. C. Polanyi and W. H. Wong, J. Chem. Phys. **51**, 1439 (1969).
[4]T. J. Odiorne, P. R. Brooks, and J. V. V. Kasper, J. Chem. Phys. **55**, 1980 (1971).
[5]D. Arnoldi and J. Wolfrum, Chem. Phys. Lett. **24**, 234 (1974).
[6]D. Arnoldi, K. Kaufmann, and J. Wolfrum, Phys. Rev. Lett. **34**, 1597 (1975).
[7]K. S. Gochelashvili, N. V. Karlov, A. I. Ovchenkov, A. N. Orlov, R. P. Petrov, Y. N. Petrov, and A. M. Prokhorov, Zh. Eksp. Teor. Fiz. **70**, 531 (1976) [Sov. Phys. JETP **43**, 274 (1976)].
[8]Z. Karny and R. N. Zare, Chem. Phys. **23**, 321 (1977).
[9]C. N. Stewart and G. Ehrlich, J. Chem. Phys. **62**, 4672 (1975); see, also, C. N. Stewart and G. Ehrlich, "Studies of Activated Chemisorption," Report R-672, February 1975, UILU Eng. 75-2206, Coordinated Science Laboratory, University of Illinois, Urbana, Illinois.
[10]J. T. Yardley and C. B. Moore, J. Chem. Phys. **45**, 1066 (1966); **45**, 2421 (1966).
[11]C. B. Moore, in *Fluorescence*, edited by G. G. Guilbault (Dekker, New York, 1967), p. 133.
[12]J. T. Yardley and C. B. Moore, J. Chem. Phys. **49**, 1111 (1968).
[13]C. B. Moore, Acc. Chem. Res. **2**, 103 (1969).
[14]J. T. Yardley, M. N. Fertig, and C. B. Moore, J. Chem. Phys. **52**, 1450 (1970).
[15]P. Zittel and C. B. Moore, J. Chem. Phys. **58**, 2004 (1972).
[16]P. Hess and C. B. Moore, J. Chem. Phys. **65**, 2339 (1976).
[17]C. B. Moore (private communication).
[18]H. F. Winters, J. Chem. Phys. **62**, 2454 (1975); **64**, 3495 (1976).
[19]H. F. Winters, J. Chem. Phys. **63**, 3462 (1975).
[20]J. T. Yates, Jr., J. J. Zinck, and W. H. Weinberg, Rev. Sci. Instrum. **50**, 132 (1979).
[21]C.-M. Chan, P. A. Thiel, J. T. Yates, Jr., and W. H. Weinberg, Surf. Sci. **76**, 296 (1978).
[22]P. A. Thiel, J. T. Yates, Jr., and W. H. Weinberg, Surf. Sci. **82**, 000 (1979).
[23]J. T. Yates, Jr., P. A. Thiel, and W. H. Weinberg, Surf. Sci. **82**, 000 (1979).
[24]J. T. Yates, Jr., P. A. Thiel, and W. H. Weinberg, Surf. Sci. (submitted for publication).

CHAPTER 3

A VERSATILE ULTRAHIGH VACUUM-MOLECULAR BEAM APPARATUS FOR SURFACE STUDIES

(The text of Chapter 3 consists of an article coauthored with W. H. Weinberg which will be submitted to *Review of Scientific Instruments*.)

Abstract

The design of an ultrahigh vacuum-molecular beam apparatus, constructed for the study of gas-surface dynamics, is described. The UHV portion of the apparatus has facilities for LEED, Auger electron spectroscopy and quadrupole mass spectrometry. The nozzle source molecular beam may be modulated by a mechanical chopper such that time-of-flight velocity analysis may be performed on the directly incident beam.

I. INTRODUCTION

This chapter describes the design of an ultrahigh vacuum-molecular beam (UHV-MB) machine, recently constructed in our laboratory **(1)**, and also serves as a manual for the use of the instrument. A review of the literature concerning the design features of nozzle source molecular beams may be obtained from Refs. 1 and 2.

Part II of this chapter details the features of the UHV chamber, in section A, and the features of the molecular beam line, in section B. Data acquisition is described in section C. Part III contains information concerning the performance of the instrument. Section A describes the method by which we estimate the intensity of a He beam used to characterize the instrument. Section B discusses time-of-flight velocity analysis for an incident He beam.

We have used the UHV-MB machine described in this chapter to perform an experiment which probes the role of translational energy in the dissociative chemisorption of CH_4 on the (110) surface of Ir. The experiment is described in Chapter 4 of this thesis.

II. SYSTEM DESCRIPTION

A. UHV system

The UHV chamber consists of three levels, as shown in Fig. 1, and has a volume of approximately 100 liters. The main chamber is pumped principally by a Balzars 2000 l/sec turbomolecular pump combined with an auxillary liquid nitrogen cooled titanium sublimation pump. The base pressure of the UHV chamber is below 2×10^{-10} torr after a 24-hour bakeout at 120°C.

1. Level I

Level I consists of a vacuum chamber the volume of which is approximately 80 cm^3 into which the sample holder may be withdrawn. At present, this coupling is used exclusively as a load lock for introducing the sample into, and retrieving the sample from, the lower levels of the UHV chamber. In the future, the cup may also be adapted to function as a high pressure microreactor, similar in design to that of Vajo et al. **(4)**. A small gate valve (Torr Vacuum Products # SVB-1.53V) can isolate the entire manipulator from the remainder of the UHV chamber when the sample is positioned at Level I, as shown in Fig. 1. This upper chamber, with the manipulator attached, may be entirely detached from the rest of the UHV system to mount and demount the sample.

2. Level II

At level II, the UHV chamber has a 23 cm radius for 210° degrees of arc, as shown in Fig. 2. A quadrupole mass spectrometer detector (EXTRANUCLEAR) has the axis of its ionizer in the horizontal level II plane, resulting in a crystal surface-to-ionizer distance of 15 cm. The quadrupole rotates in an arc subtending 190° about the sample position, as shown in Fig. 2, and described in more detail in subsection 5 (Rotating Seal). It is possible to position the quadrupole such that the velocity distribution of the directly incident beam may be characterized when the sample is raised out of the path of the beam. At present, the quadrupole is not differentially pumped.

The UHV chamber truncates to 13 cm in its remaining 150° of arc at level II, as shown in Fig. 2. This truncation permits low-energy electron optics (LEED; Varian # 981-2158), designed for a flange face to sample distance of 25 cm to be mounted at level II. The LEED optics are mounted on a bellows (not shown in Fig. 2) so that they may be moved up to 13 cm away from the

sample during a molecular beam scattering experiment.

A miniature pnuematic gate valve is mounted inside the UHV chamber at Level II, as shown in Fig. 2. This valve provides isolation of the molecular beam line from the UHV chamber, without increasing the beam source-to-sample distance, and has been described in detail elsewhere **(5)**.

3. Level III

The entire UHV chamber has a 13 cm radius at level III. A double pass cylindrical mirror analyzer (DPCMA; PHI # 15-255G) and a sputter ion gun (PHI # 04-161) are mounted at this level. At present, we are capable of performing Auger electron spectroscopy (AES) only. However, the UHV chamber has been designed to accommodate the addition of both an X-ray photoelectron spectroscopy (XPS) source (PHI # 1250), and an ultraviolet photoelectron spectroscopy (UPS) source (PHI # 1500) source, compatible with the DPCMA, in the future.

4. Sample Manipulator

The sample manipulator is custom designed to allow the sample to be positioned at each level of the UHV chamber, and has been described in detail elsewhere **(6)**. Briefly, the manipulator is capable of 56 cm of vertical translation, 2.5 cm of horizontal movement in two perpendicular horizontal directions and 360° of independent polar and azimuthal rotation of the sample. A gimbals assembly provides a tilt for the sample. The manipulator provides facilities for resistive heating and cryogenic cooling of the sample. We have successfully employed this manipulator at sample temperatures from 130 K to 1600 K, as measured by a W/5%Re / W/26%Re thermocouple spotwelded to the back of the sample, in this case a single crystal of iridium.

5. Rotating Seal

The lid of the bell jar, upon which the sample manipulator and the quadrupole mass spectrometer detector are mounted, is a rotatable shaft, 46 cm in diameter, which follows the design of Auerbach et al. **(7)**, and which is shown in Fig. 3. The shaft is supported by a single roller bearing (Kaydon Bearing # KD180XPO) and seals against three spring-loaded teflon O-rings (Accratronics # A03002) which define two regions of differential pumping. The first region is pumped by a 20 l/min mechanical pump to a pressure of approximately 0.2 torr. The second region is pumped by a 20 l/sec ion pump to a pressure typically in the high 10^{-8} torr range.

A pressure rise of 2×10^{-10} torr is noted when the seal is rotated at an angular velocity of 1 degree/sec. However, the base pressure is regained seconds after the seal has stopped moving.

B. Molecular Beam Line

The molecular beam line consists of three chambers, numbered 1, 2, and 3 in Figs. 1 and 2, each of which is separately pumped. Beam chamber 1 is the source chamber, in which the molecular beam is formed by expansion of the source gas through a nozzle,and which will be described in more detail below. Beam chambers 2 and 3 are buffer chambers, used to reduce the background pressure of gas produced as a result of collimation of the beam. These buffer chambers prevent an unacceptably high pressure of background gas from diffusing into the UHV chamber during operation of the beam. A typical set of operating conditions is given in Table 1.

Beam chambers 1 and 2 are demountable, but beam chamber 3 is integral to the UHV system, as shown in Fig. 2. Dowel pins fixed in the beam chamber flanges facilitate reassembly following demounting of beam chambers 1 and

2 , for example, to vary aperture sizes, or after performing any maintenance which may be required.

1. Beam Chamber 1

Beam chamber 1 comprises the upper section of a 20 cm O.D. vacuum cross, which is partitioned into an upper and lower chamber, as shown in Fig. 1. A 25 cm I.D., inverted U shaped vacuum coupling connects beam chamber 1 with a 6" oil diffusion pump (CVC Blueline # PMC-6B), which has a pumping speed of 1600 l/sec for H_2. A Millitorr gauge (Varian # 971-5009) is available on the vacuum coupling for measurement of the pressure in chamber 1. A conical skimmer (Beam Dynamics Type 1) is mounted in beam chamber 1, and is the collimating orifice through which the molecular beam enters chamber 2. At present, a skimmer having an orifice diameter of 2 mm is mounted in beam chamber 1, however; we have the flexibility to substitute skimmers of different orifice sizes.

2. Beam Chamber 2

The lower section of the 20 cm O.D. vacuum cross is connected directly to an oil diffusion pump (Edwards Diffstak 160P) with a pumping speed of 1300 l/sec for H_2. An ionization gauge (Varian # 971-5008) is mounted on the lower section of the vacuum cross, for measurement of the pressure in beam chamber 2. Beam chamber 2 is isolated from chamber 3 by an extension tube welded to a 20 cm O.D. double knife edge flange, as shown in Figs. 1 and 2. A collimating aperture, the size of which may be varied, and through which the molecular beam passes into chamber 3, is mounted on the front face of the extension tube, as shown in Figs. 1 and 2. At present, we are using a collimating aperture of 6 mm diameter. The distance between the skimmer orifice and the collimating aperture is 15.0 cm.

3. Beam Chamber 3

Beam chamber 3 is pumped by a turbomolecular pump (Balzars # TPH 110) which has a pumping speed of 110 l/sec for H_2. A final collimating aperture, of 0.6 cm diameter (the size of which may be varied), is mounted between chamber 3 and the gate valve opening to the main chamber, as shown in Figs. 1 and 2. The distance between the collimating apertures of beam chambers 2 and 3 is 8.9 cm. A mechanical chopper, for incident beam modulation, is also mounted in beam chamber 3, and will be discussed in more detail below.

The total source-to-sample distance is 37.2 cm, when the sample is positioned in the center of the UHV chamber, and the nozzle is positioned 0.6 cm from the skimmer orifice. The distance from the chopper blade to the center of the ionizer of the quadrupole mass spectrometer detector is 28.8 cm.

4. Nozzle Source

We are presently using quartz nozzle sources in our molecular beam line, which were fabricated from 0.69 cm O.D. x 0.47 cm I.D. quartz tubes. The tubes are drawn to a "point" at one end, and this "point" is mechanically ground to produce an orifice size that is typically in the range of 20-100 microns. The size of the orifice is established by viewing the ground end of the quartz tube under a microscope (Titan Tool Supply # 72A) at X100 magnification.

The quartz tube is mounted in an ULTRA-TORR (8) fitting, which is attached to a vacuum flange. This flange mounts directly on a manipulator designed to allow the quartz tube to be moved in line with the skimmer **(1)**. A 20 cm O.D. viewport, mounted directly above the nozzle-skimmer system,

allows a rough, lateral positioning of the nozzle. The final position of the nozzle is determined by maximizing the signal of an electrometer, that is coupled to the output of the quadrupole mass spectrometer detector, while adjusting the nozzle manipulator.

5. Beam Modulation

The incident beam is modulated by a single-shot rotating blade chopper mounted in beam chamber 3. The chopper blade is mounted on a miniature, variable frequency, hysteresis-synchronous motor (Globe # 75A1003-2). The motor is equipped with vacuum compatible bearings (Globe # 15D134) which have MoS_2 filled teflon ball separators but no other lubrication. A water jacket encloses the motor in order to cool it during operation, and to cool it during system bakeout. The motor is supported by a split clamp assembly which encircles the water jacket. This assembly is coupled to a linear motion feedthrough which allows the whole assembly to be moved vertically with respect to the beam axis. The chopper assembly is illustrated schematically in Fig. 4. The modulation frequency of the beam is variable between 200 and 1600 Hz.

The chopper blade, a machined metal disk of 7.6 cm diameter, is designed so that the beam may be sampled in either a 0.2% duty cycle or a 25% duty cycle, depending on the vertical height of the blade with respect to the beam. This allows us to perform time-of-flight velocity analysis of the directly incident beam with on the order of 5 μsec time resolution, or when such time resolution is not required, to increase our rate of data acquisition without breaking vacuum in the molecular beam line to change chopper blades.

There are an even number of windows machined into the chopper blade, arranged symmetrically. This arrangement ensures that when a window

crosses the molecular beam, a window will also pass between an LED and a photodiode which are mounted on the chopper assembly, as shown in Fig. 4. Data acquistion, as described in more detail below, is initiated by a signal from the photodiode.

Errors in timing can be caused by misalignment of the blade windows with respect to the beam and the photodiodes. The amount of misalignment can be measured, and corrected for in data analysis, by comparing data aquired for clockwise and counter clockwise rotation of the chopper blade.

C. Data Aquisition

The quadrupole mass spectrometer detector is interfaced to a high speed CAMAC system for signal averaging. The output of the electron multiplier (EXTRANUCLEAR # 047-72) is input to a counting preamplifier (EXTRANUCLEAR # 032-3). The output from the preamp is fed to a 50 ohm driver to produce TTL pulses compatible with the signal input of a CAMAC multichannel scalar (Lecroy # 3521). When a window of the chopper blade passes through the molecular beam, another window on the blade simultaneously passes between a vacuum compatible photodiode (Motorola # MRD500) and a vacuum compatible LED (Motorola # MLED930). The output pulse of the photodiode is passed through a 50 ohm driver and subsequently connected to the trigger input of the multichannel scalar in order to begin data aquisition.

III. SYSTEM PERFORMANCE

A. Measurement of the Unmodulated Beam Signal Intensity

Operating conditions for a He beam, used to characterize the performance of the instrument, are given in Table I. A measure of the effective pressure of the unmodulated beam at the detector was obtained by observing the resi-

dual gas mass spectrum with the detector both directly in line, and out of line, with the incident beam. The total pressure of the UHV chamber, as measured with an ionization gauge (Varian # 971-5008) during the beam experiment, was compared to the partial pressures of the components of the residual gas mass spectrum, correcting for ionization efficiencies. The effective pressure of the He beam measured in this way was on the order of 5 x 10^{-7} torr.

B. Time-of-Flight Velocity Analysis of the Incident Beam

A time-of-flight spectrum of a He beam with a velocity distribution of 11% is shown in Fig. 5. Since obtaining this spectrum (11-16-84) we have increased our beam signal 100 fold, i.e. to the level described in Section A above. Unfortunately, technical difficulties have prevented us from obtaining more recent TOF spectra of the more intense beam, which we expect to have a more narrow velocity distribution than that displayed in Fig. 5.

IV. CONCLUSIONS

An ultrahigh vacuum-molecular beam apparatus has been designed and constructed. The instrument has been tested and characterized using a He beam. The role of translational energy in the dissociative chemisorption of CH_4 on the (110) surface of Ir has been investigated with this apparatus, as described in Chapter 4 of this thesis.

Table 1.
Typical Operating Conditions for the UHV-MB Machine

Beam source gas: He

Beam source pressure: 26 psia

Quadrupole mass spectrometer emission current: 0.1 mA

Quadrupole mass spectrometer multiplier high voltage: 2900 eV

Quadrupole mass spectrometer electrometer signal current: 8×10^{-9} Amps

Quadrupole mass spectrometer electrometer input resistance: $8 \times 10^{7}\Omega$

	Beam on[c]	Beam off[c]
Pressure[a] in beam chamber 1:	1×10^{-4}	7×10^{-6}
Pressure[b] in beam chamber 2:	5×10^{-6}	2×10^{-7}
Pressure[b] in beam chamber 3:	3×10^{-6}	1×10^{-6}
Pressure[b] in UHV chamber:	5×10^{-9}	2×10^{-10}

[a]As measured by a Varian millitorr gauge, mounted on the chamber.

[b]As measured by a Varian ionization gauge, mounted on the chamber.

[c]All pressures in torr.

References

1. J. J. Zinck and W. H. Weinberg, in preparation.

2. P. P. Wegener, 'Molecular Beams and Low Density Gasdynamics", Marcel Dekker Inc., NY, 1974.

3. T. Engel and K. H. Rieder, Springer Tracts in Modern Physics **91**, 55 (1981).

4. J. Vajo, W. Tsai and W. H. Weinberg, to be published in Rev. Sci. Instrum.

5. J. J. Zinck and W. H. Weinberg, Rev. Sci. Instrum. **55**, 810 (1984), and Appendix C of this thesis.

6. J. J. Zinck and W. H. Weinberg, to be published in Rev. Sci. Instrum., and Appendix B of this thesis.

7. D. J. Auerbach, C. A. Becker, J. P. Cowin and L. Wharton, Rev. Sci. Instrum. **49**, 1518 (1978).

8. ULTRA-TORR is a registered trademark of Cajon Vacuum Products, 9760 Shepard Road, Macedonia, Ohio 44056.

Figure Captions:

Fig. 1. Cross-sectional view of the ultrahigh vacuum-molecular beam apparatus. a) Sample holder. b) Low-energy electron diffraction optics. c) Double pass cylindrical mirror electron energy analyzer. d) Quadrupole mass spectrometer detector. e) Cryostat tube of sample manipulator. f) Gate valve; Torr Vacuum, manual. g) Rotating seal. h) Gate valve; Huntington, modified, pneumatic. i) Gate valve; Torr Vacuum, pnuematic. j) Pump; liquid nitrogen cooled Ti sublimation. k) Pump; Balzars, turbomolecular. l) Vacuum gauge; Varian, cold cathode. m) Support for UHV chamber. n) Chopper motor. o) Quartz nozzle. p) Skimmer. q) Collimating aperture; beam chamber 2→3. r) Collimating aperture; beam chamber 3→UHV. s) To pump; Edwards, oil diffusion. t) To pump; Balzars, turbomolecular. u) Bellows of vacuum coupling from beam chamber 1 to CVC oil diffusion pump. v) Viewport. w) To pump; CVC, oil diffusion. x) Nozzle manipulator. y) Source gas connection location.

Fig. 2. Cross-secctional view of level II of the ultrahigh vacuum-molecular beam apparatus. a) Quartz nozzle. b) Skimmer. c) Collimating aperture mount; beam chamber 2→3. d) Collimating aperture mount; beam chamber 3→UHV. e) Gate valve; modified, Huntington, pneumatic. f) Sample holder. g) Quadrupole mass spectrometer detector. h) Laser; He/Ne, alignment. i) Viewport. j) Vacuum coupling; beam chamber 1 to CVC oil diffusion pump. k) Low-energy electron diffraction

port. l) Nozzle manipulator port.

Fig. 3. Cross-sectional view of the rotating seal.

Fig. 4. Cross-sectional view of the chopper assembly. a) Chopper motor. b) Water cooling jacket. c) Split clamp. d) Chopper blade. e) Screw. f) LED. g) Photodiode. h) Platform. i) Bearing shaft. j) Bearing shaft guide. k) Linear motion feedthrough shaft. l) Vacuum face of chopper assembly flange.

Fig. 5. Time-of-flight spectrum of an incident He beam from a quartz nozzle having an orifice diameter (d_N) of 50 microns and a source pressure (P_0) of 30 psia.

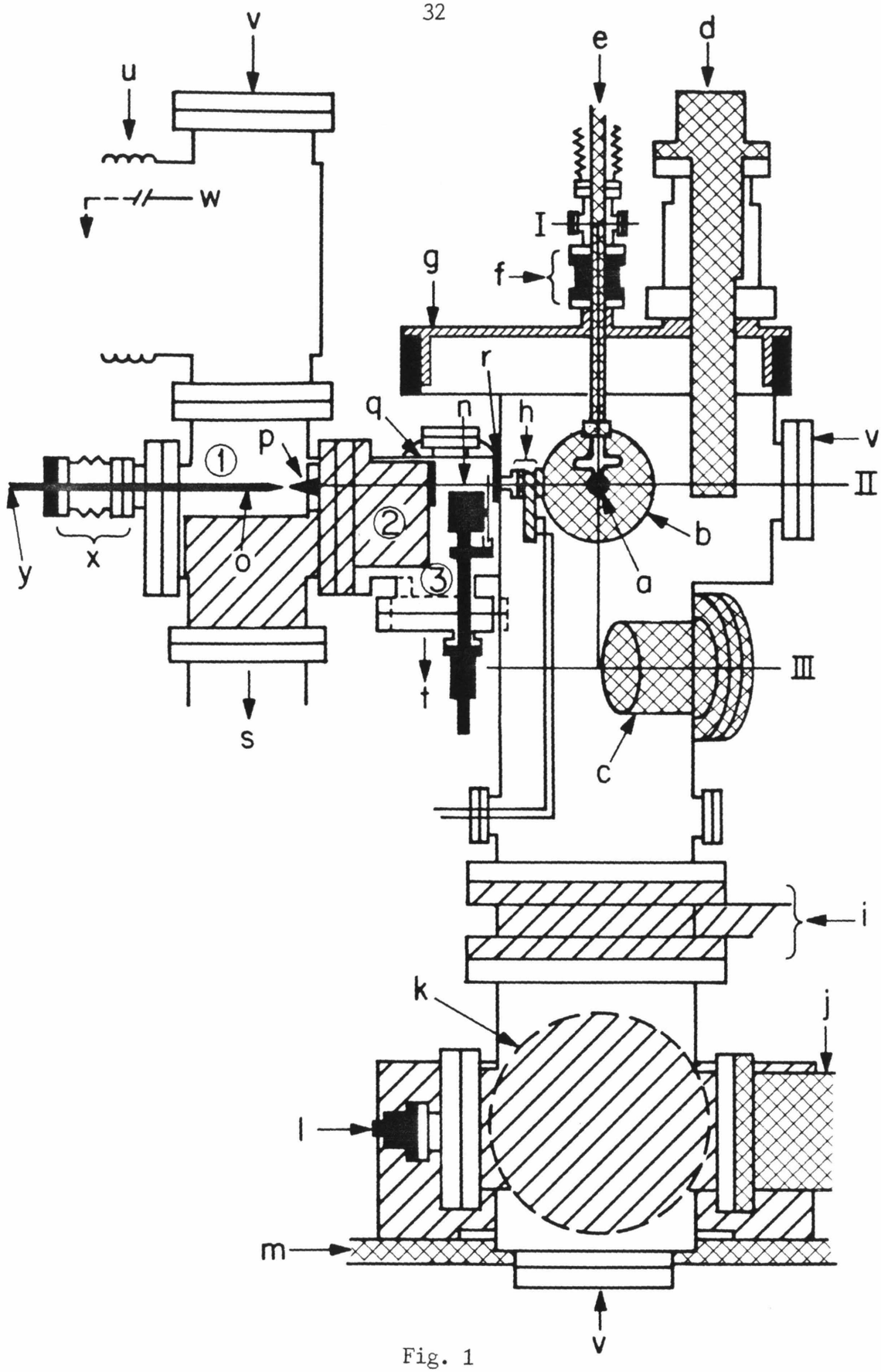

Fig. 1

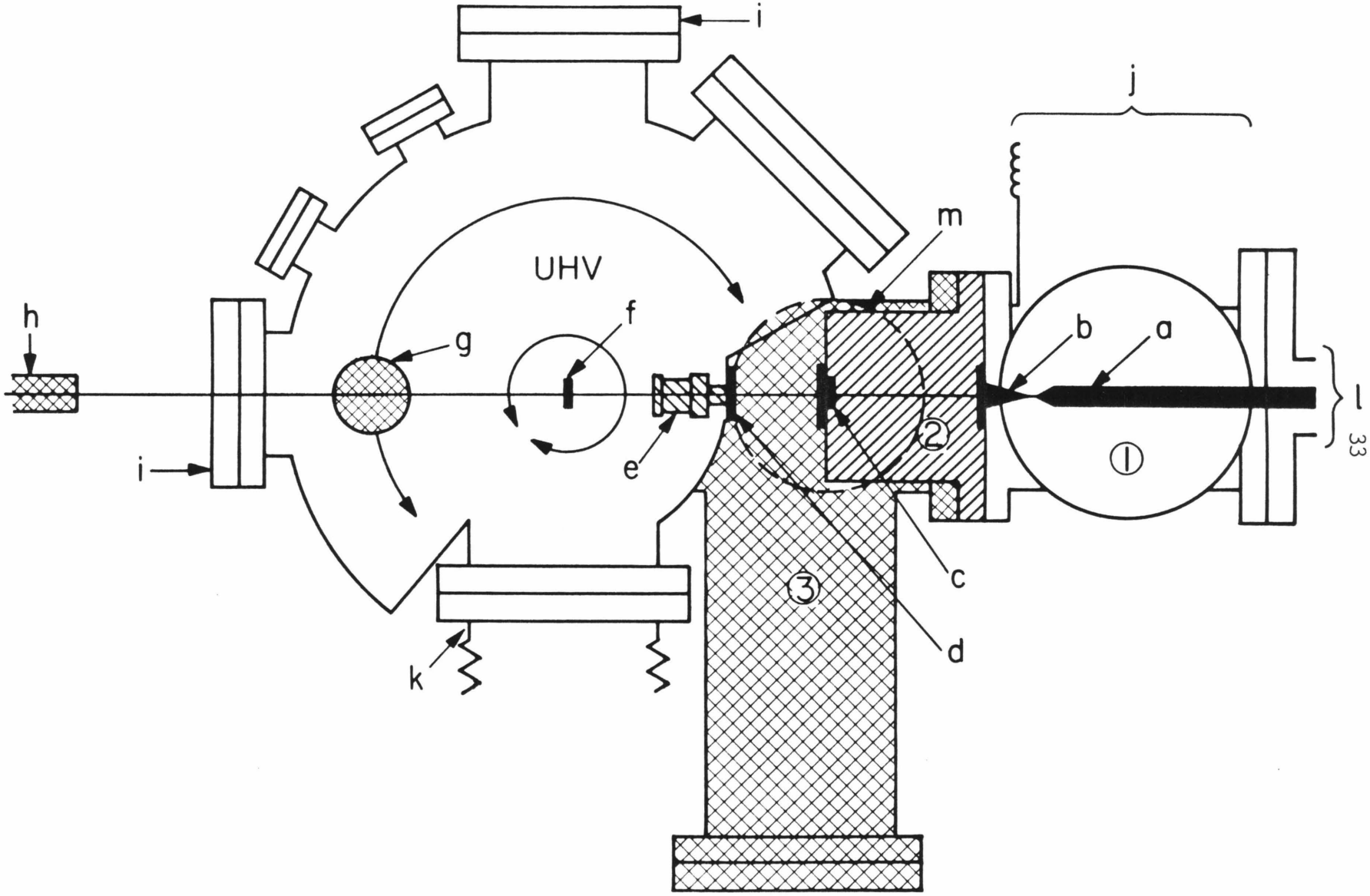

Fig. 2

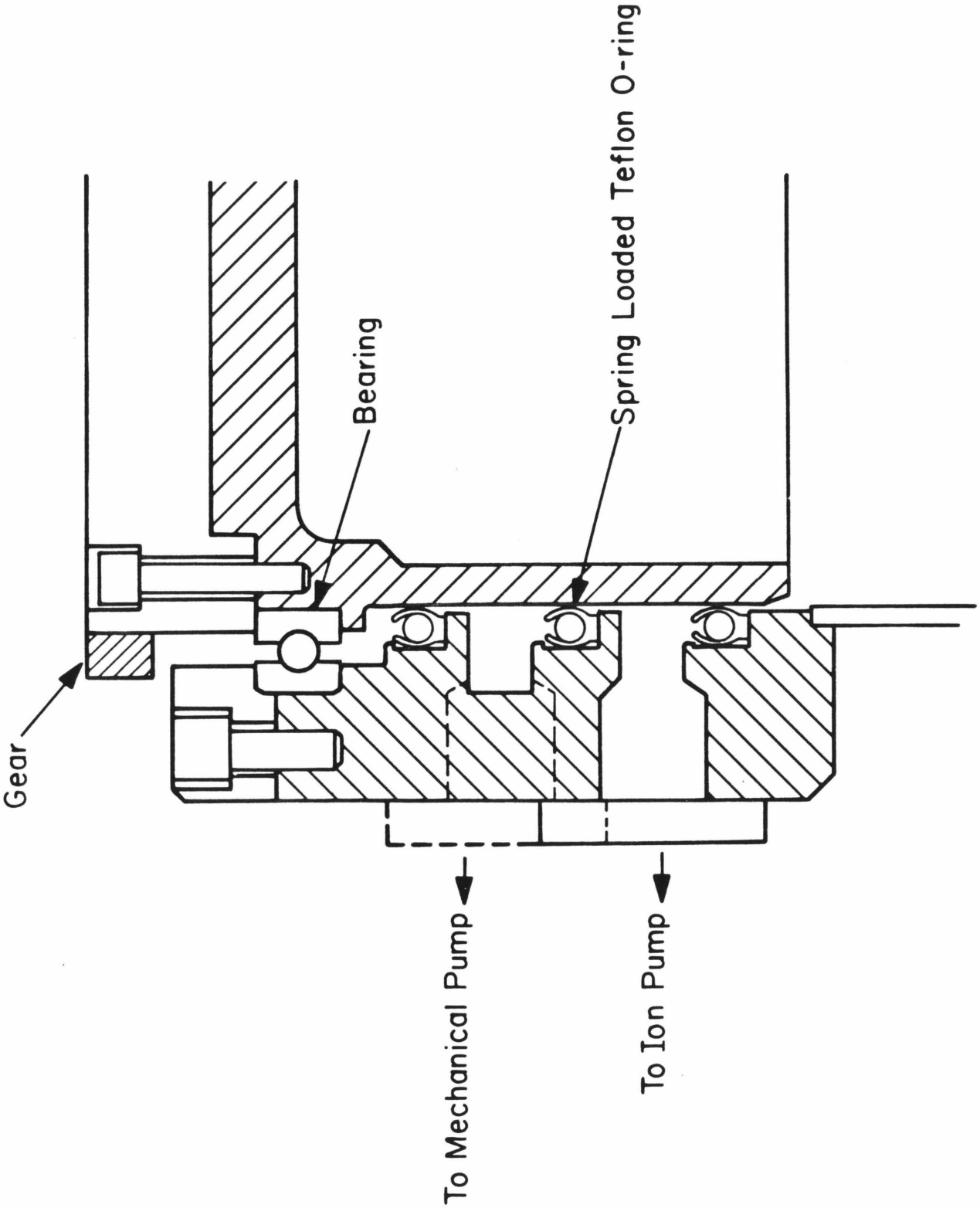
Gear
Bearing
Spring Loaded Teflon O-ring
To Mechanical Pump
To Ion Pump

Fig. 3

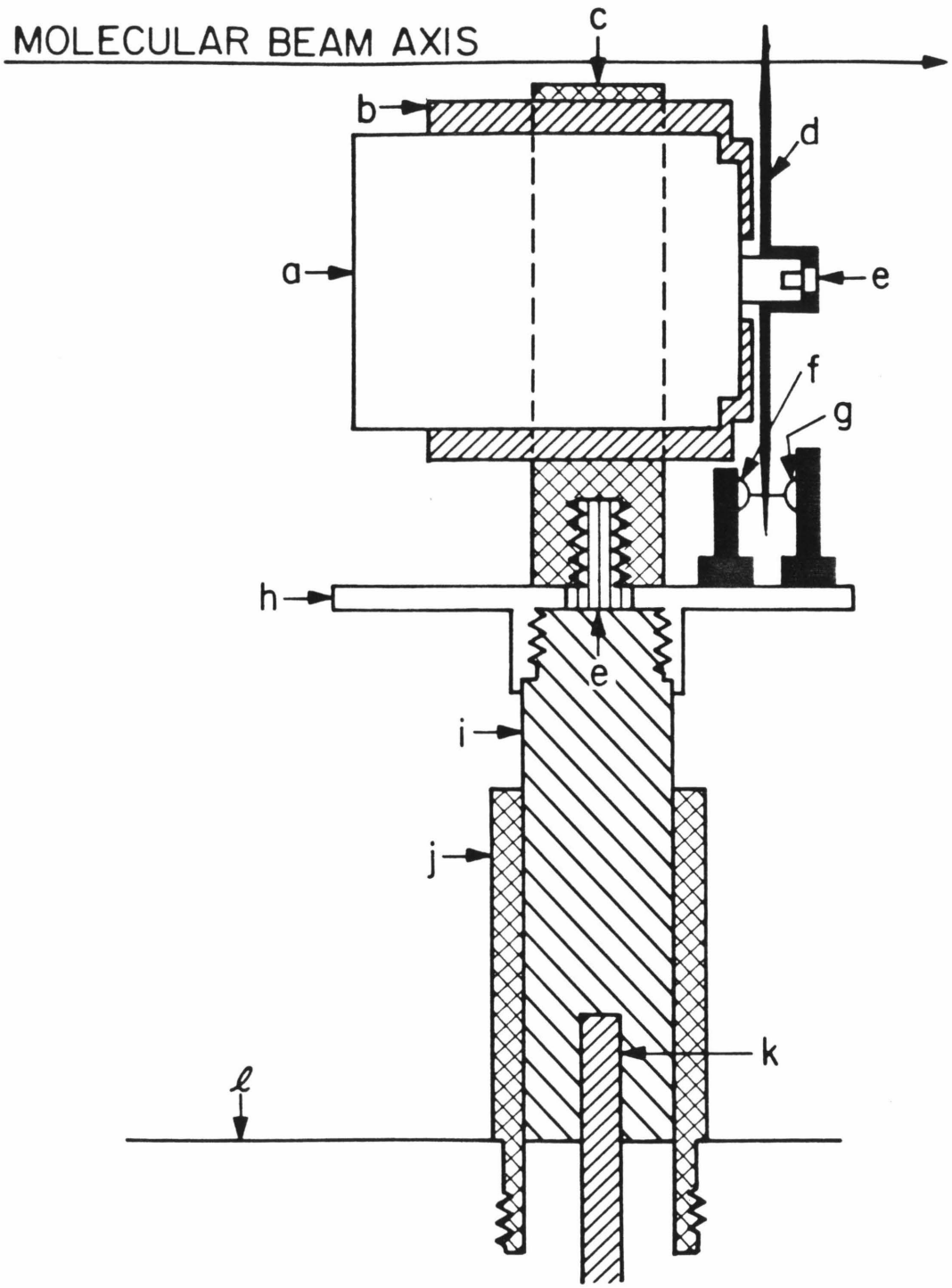

Fig. 4

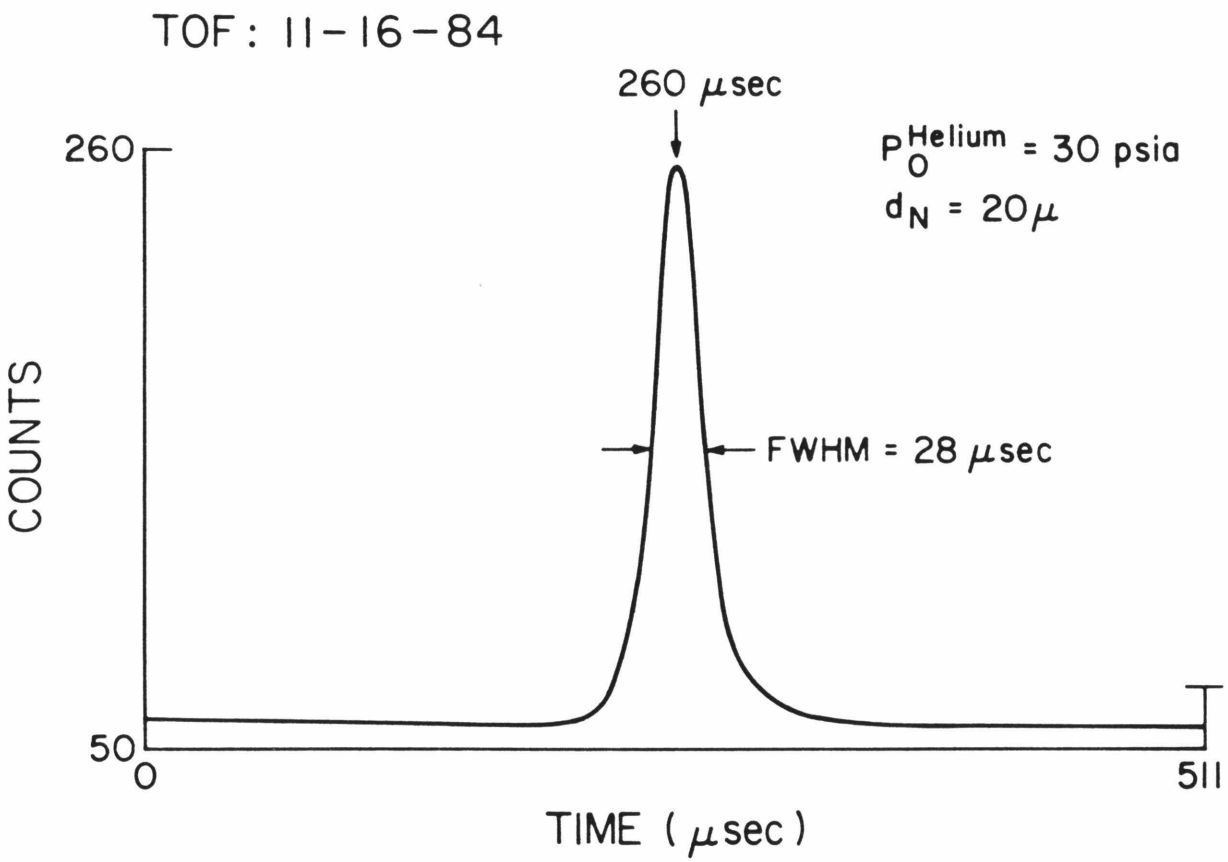
TOF : 11-16-84
260 μsec
260
P_0^{Helium} = 30 psia
d_N = 20μ
FWHM = 28 μsec
COUNTS
50
0
511
TIME (μsec)

Fig. 5

CHAPTER 4

THE ROLE OF TRANSLATIONAL ENERGY IN THE DISSOCIATIVE CHEMISORPTION OF METHANE ON THE Ir(110)-(1x2) SURFACE

Abstract

The role of translational energy in the chemisorption of CH_4 on the (110) surface of Ir is studied using molecular beams of CH_4 seeded in He and H_2. Dissociation of CH_4 on the surface of 700 K is determined by CO temperature programmed desorption measurements. A dissociation probability of $< 2 \times 10^{-4}$ is measured for CH_4 having an average translational energy of 10 kcal/mole.

I. INTRODUCTION

Considerable interest has been directed recently toward the topic of C-H bond activation in alkanes **(1-3)**. Alkanes are a potentially useful resource, from which other chemicals can be synthesized. However, a suitable catalyst must be found which can lower the activation barrier to dissociation of the C-H bond, while retaining selectivity for a particular reaction pathway.

Both homogeneous **(1)** and heterogeneous **(2,3)** catalysts are being explored as possible solutions to this problem. Recently, some success has been experienced in homogeneous work, using particular organometallic dihydride complexes of Ir **(4)**, and Rh **(5,6)**. Ultraviolet irradiation of these dihydridometal complexes generates an intermediate which reacts rapidly with C-H bonds. In the area of heterogeneous catalysis, the traditional approach has been to study the reaction of alkanes at high pressures over supported transition metal catalysts such as, for example, Rh and Ir, which are known dehydrogenation, hydrogenation and hydrogenolysis catalysts. Since the development of ultrahigh vacuum techniques (UHV), there have been many studies of the chemisorption of alkanes on transition metal surfaces in UHV **(3)**. Alkane dissociation on transition metal surfaces has been observed to be activated. On the Ir(110)-(1x2) surface, the apparent activation barrier to dissociation of ethane, propane, isobutane and neopentane is approximately 7 kcal/mole **(7)**. This chapter deals with an attempt to understand the dynamics of activated adsorption of CH_4 on the Ir(110)-(1x2) surface.

An experiment is described in which a nozzle source molecular beam of CH_4, incident upon a reconstructed Ir(110)-(1x2) surface in UHV, is used to probe the role of translational energy in the dissociative chemisorption of

CH_4. The chapter is organized in the following way. Part I gives a brief synopsis of the literature concerning the chemisorption of CH_4 on transition metal surfaces in UHV. Part II contains a description of the experimental method employed to test the role of translational energy in the chemisorption of CH_4 on the Ir(110)-(1x2) surface. Part III contains the results obtained in the experiment to be described in Part II, and discusses these results in comparison to those of analogous systems. Lastly, section IV describes a program of future work for the CH_4/Ir(110)-(1x2) system.

A. The Chemisorption of CH_4 on Group VIII Transition Metals, Studied in UHV

A survey of the literature available concerning the dissociative chemisorption of CH_4 on transition-metal surfaces in UHV is given in Table 1. In general, except for the work of Rettner et al. **(8)**, the extent of dissociative adsorption of CH_4 observed on these surfaces is small. Yates and Madey have observed that CH_4 will adsorb molecularly on W(100) into a presumably physically adsorbed state of binding energy 6.9 kcal/mole, when the surface temperature is 77 K **(9)**. However, they observe no measurable dissociation of CH_4 from this state. Yates et al. have also shown **(10)** that no measurable enhancement of the dissociation of CH_4 on Rh(111) is observed when CH_4 is excited to its ν_3, $2\nu_4$ or ν_4 vibrational states, in contradiction to the model for dissociative chemisorption of CH_4 on Rh proposed by Stewart and Ehrlich **(11)**. (Reference 10 comprises Chapter 2 of this thesis.)

The recent data of Rettner et al. **(18)** suggest that increasing the normal component of translational energy of CH_4, i.e. the normal component as defined by the direction of a molecular beam of CH_4 with respect to the plane of the surface, results in an increase in the initial probability of adsorption

of CH_4 on W(110) of approximately 5 orders of magnitude. Rettner et al. propose a chemisorption mechanism which is dominated by quantum tunneling, a model which has also been proposed previously by Winters **(12,13)**

We are presently performing an analogous experiment to that of Rettner et al. using seeded molecular beams of CH_4 incident upon the reconstructed Ir(110)-(1x2) surface.

B. The Ir(110)-(1x2) Surface

Christmann and Ertl **(14)** were the first to report that the clean (110) surface of Ir reconstructs to a (1x2) structure, where the lattice parameter in the [001] direction is twice that of the bulk lattice. The structure of the reconstructed surface has been analyzed by low-energy electron diffraction (LEED) **(15)** and the data agree best with a missing row model, where every other row of the topmost layer of atoms is missing, as shown in Fig. 1. The resultant surface is highly corrugated on a microscopic scale, and consists of two-layer deep troughs, the sides of which are (111) microfacets. Wittrig et al. **(16)** have observed that the reconstruction is stable from 130 K to 1300 K, in the presence of a carbonaceous residue resulting from hydrocarbon decomposition on the surface.

II. EXPERIMENTAL

The ultrahigh vacuum molecular beam apparatus, with which the experiment has been performed, is described in detail in Chapter 2 of this thesis.

A. Establishing a Clean, Reconstructed Ir(110)-(1x2) Surface

The Ir crystal, a roughly circular disk of 6 mm diameter and 0.5 mm thickness, was cut and polished by standard techniques **(17)**. Auger electron spectroscopy (AES) of the crystal in UHV indicated that, initially, more than

a monolayer of C was contaminating the surface, i.e. no Auger peaks of Ir were found in the AES spectrum as shown in Fig. 2a. It was necessary to Ar ion bombard the surface and subsequently expose the surface to O_2 at a crystal temperature of 600 K, before Ir features could be identified by AES **(18)**. After ion bombardment, it was necessary to anneal the crystal at 1600 K to order the surface, and in consequence, C diffused from the bulk of the crystal to the surface, as shown by the subsequent AES spectrum. An AES spectrum of the carbon contaminated Ir surface is displayed in Fig. 2b. Exposures of the crystal to oxygen at 10^{-7} torr for 1/2 hour periods, with the crystal held at 600 K, followed by a flash to 1600 K, were repeated until no C was observed in the AES spectrum. After cleaning, the extra spots of the (1x2) reconstruction could be observed in the LEED pattern, appearing as streaks in the [001] direction, with the crystal temperature at 300 K. An AES spectrum of the clean Ir surface is displayed in Fig. 2c.

B. Preparation of Seeded Methane Mixtures in He and H_2

When a molecule of mass m_s is seeded dilutely in a carrier gas of mass m_c and expanded through a nozzle, the velocity of the seeded particles will approach that of the pure carrier gas **(19)**, i.e.,

$$v_s^2 = v_c^2 = 2\bar{\gamma}kT/(\bar{\gamma} - 1)\bar{m} \tag{1}$$

$$\bar{\gamma} = X_s\gamma_s + X_c\gamma_c \tag{2}$$

$$\bar{m} = X_s m_s + X_c m_c \tag{3}$$

$\bar{\gamma}$ = average ratio of specific heats

X = mole fraction

$\bar{m}$ = average mass

In this experiment we have studied the three mixtures 1% CH_4/He, 11% CH_4/H_2, and 1% CH_4/H_2. The average translational energies of CH_4 molecules in the beam, corresponding to each of these mixtures, are 5.5, 9.6 and 16.5 kcal/mole, respectively, as shown in Table 2. To date, time-of-flight (TOF) spectra are not available to confirm these calculations.

Matheson research purity CH_4 (99.99%), Matheson ultrahigh purity He (99.999%) and H_2 (99.995%) were used to make the gas mixtures, without further purification. After preparing a mixture, which was stored at several hundred psig in a commercial (size 1A) cylinder, the base of the storage cylinder was wrapped with heating tape and the vessel warmed for at least 12 hours. This procedure has been claimed to be necessary for complete mixing of the CH_4 and the lighter carrier gas **(20,21)**.

C. Alignment of the Crystal Surface in the Beam

The crystal surface is aligned such that the surface normal is coincident with the beam axis with the assistance of a Coherent 1105p (5 mW) He/Ne laser. The laser is positioned such that it passes through the exit, and then the entrance, apertures of a quadrupole mass spectrometer detecter, and is focused on the third beam chamber aperture with the beam isolation valve open, as shown in Fig. 3. The quadrupole is in line with the beam so that, when the crystal manipulator has been raised out of the way, the incident beam can be characterized directly. It is possible to see the laser light strike the tip of the quartz nozzle, via a plexiglass viewport mounted on the first beam chamber above the nozzle-skimmer system. After the laser beam has been correctly positioned, the sample manipulator is lowered until the laser beam can be seen to strike the back of the sample holder. The manipulator is than adjusted using its XY translators to center the laser spot with respect

to the crystal.

In addition to the laser alignment, the alignment of the crystal in the beam was confirmed by exposing the crystal for 10 seconds to a pure hydrogen beam, followed by a H_2 temperature programmed desorption (TPD) measurement. A blank experiment was performed in which the crystal surface was turned 180° away from the incident beam. The sample manipulator shields the back face of the sample, such that there is no line of sight for the beam to the Ir crystal. An increased H_2 TPD area, with respect to that measured in the blank experiment, was evidence that the beam was hitting the sample.

The beam cross-sectional area at the crystal has been observed to be approximately 10% of the area of the crystal. For this measurement, a viewport was substituted for the nozzle flange, and with both the UHV system and the beam line under vacuum, the light from an incandescent source, placed behind the viewport, could be seen on the crystal.

D. Experimental Procedure: CH_4/Ir(110)-(1x2)

We have used CO (TPD) to monitor the decomposition of CH_4 on the Ir(110)-(1x2) surface. It should be noted that CO produced via the reaction of adsorbed carbon atoms with adsorbed oxygen atoms is distinguishable from the desorption of molecularly adsorbed CO, as shown in Fig. 4 **(22)**. However, our exposures of the surface to the beam were long (900-2700 seconds), and we therefore maintained the crystal temperature above the desorption temperature of CO (700 K maximum) to minimize background contamination of the clean surface. CO has been observed to have an initial sticking probability of unity at 300 K on the Ir(110) surface **(23)**, as does H_2, which desorbs from the Ir(110)-(1x2) surface below 500 K **(24)**.

The experimental procedure used is outlined below, and is displayed schematically in Fig. 5. A blank experiment consisted of the same experimental steps a-h, but with the surface rotated 180° from the incident beam.

a. With the beam isolation valve closed, a stagnation pressure P_0 = 25-45 psia was admitted to the quartz nozzle, and time was allotted to allow the source gas lines to be flushed of contaminants.

b. The crystal was cleaned according to the following prescription. The sample was heated to 700 K to desorb CO and H_2. The sample was subsequently exposed to 20 L O_2 (1 Langmuir, L, = 10^{-6} torr-sec) followed by a flash of the crystal temperature to 1600 K.

c. The crystal temperature was cooled and stabilized at 700 K.

d. The beam isolation valve was opened, and the Ir surface was exposed to the beam for 900-2700 seconds.

e. The beam isolation valve was closed, and the crystal was cooled to 400 K.

f. After cooling to 400 K, the surface was exposed to 20 L of O_2.

g. The crystal was flashed to 1200 K at a heating rate of 25 K/second, and the CO TPD was recorded.

h. The crystal was flashed to 1600 K to remove residual surface O_2.

III. RESULTS AND DISCUSSION

A. Results

The probability of dissociation of CH_4 is defined here as the ratio of the number of molecules associated with the measured CO TPD area with respect to the number of CH_4 molecules directly incident on the Ir(110)-(1x2) surface at 700 K. This quantity is plotted as a function of the average transla-

tional energy calculated for the seeded beam mixtures, and is displayed in Fig. 6. Within the error of our measurements, no correlation can be claimed for these data. More work is needed to establish the role of translational energy in the dissociative adsorption of CH_4 on the Ir(110)-(1x2) surface.

However, if we consider only the 11% CH_4/H_2 mixture experiment, for which we have several data points, the average value of 2×10^{-4} obtained for the probability of dissociative adsorption of CH_4 may be used to calculate a lower limit to the energy of the barrier on the Ir(110)-(1x2) surface.

B. Calculation of a Lower Limit to a Translational Energy Barrier

In this calculation, it has been assumed that the translational energy distribution of the CH_4 molecules in the beam may be described by the normal distribution function. Assuming this, then the probability that a CH_4 molecule in the beam has translational energy greater than some value E is

$$P(E) = 1/\sqrt{2\pi} \int_{E}^{+\infty} e^{-x^2/2} dx \quad x = ((E' - \bar{E})/\sigma) \tag{4}$$

where E' is the translational energy, $\bar{E}$ is the average value of the translational energy and σ is the standard deviation of the distribution, calculated using the average value and the full width at half maximum (FWHM) of the distribution, as measured in a TOF spectrum.

Estimates for $\bar{E}$ and σ were obtained by making the following assumptions:

i. The FWHM is 20% of $\bar{E}$ (This is based on measured TOF spectra for He beams, where we routinely obtained velocity distributions of ± 5% of $\bar{v}$).

ii. $\bar{E} = (1/2)mv_s^2$, where v_s is calculated using Eq. (1) of this chapter.

A lower limit of approximately 13 kcal/mole for an energy barrier to the dissociative adsorption of CH_4 on the Ir(110)-(1x2) surface is calculated using the average of the measured dissociation probabilities, 2×10^{-4}, associated

with a beam of CH_4 molecules having an average translational energy of approximately 10 kcal/mole.

C. Discussion

In this section, processes that may occur during the experiment, but were not considered in the preceding analysis, are discussed in terms of their effect on the results presented in the previous section.

At an Ir crystal temperature of 700 K, it is most likely that the dominant mechanism of any CH_4 dissociation on the surface is thermal activation over the energy barrier. Tunneling of an H atom to produce an adsorbed CH_3 group and an adsorbed H atom may not be precluded, à priori. However, Difaggio and Gomer have reported **(23)** that in the activated diffusion of H atoms on a W(110) surface, tunneling is only important at surface temperatures below 160 K, and that the transition to a thermally activated mechanism for H adatom diffusion is abrupt. The presence of tunneling would not affect the result of Section IIIB, of a lower limit to a translational energy barrier.

It is known **(26)** that in the case of W surfaces, WC forms at temperatures as low as 800 K, and is complicated by adsorption of carbon onto the carbide as well as diffusion of C into the bulk. Nickel has also been observed to form a surface carbide at temperatures above 600 K, and there is evidence of C diffusion from the surface into the bulk **(27,28)** also. If C from dissociatively adsorbed CH_4 on the Ir(110)-(1x2) surface became incorporated in an interstitial carbide or diffused into the bulk of the Ir crystal, it would not be detected in this experiment. AES detection of surface C would be a useful addition to the experimental procedure, and is suggested for future work.

IV. FUTURE WORK

A. Heating the Beam Source

In order to probe further the role of translational energy in the dissociative chemisorption of CH_4 on the Ir(110)-(1x2) surface, we must heat our beam source. A very simple heater, consisting of a 2" length of thermocoax **(29)** wire wound to slip fit the O.D. of the quartz nozzle source tube, has already been fabricated and is ready for testing in our laboratory. A similar heater has been tested in another laboratory at Caltech **(30)**, and it was claimed that gas temperatures of 1000 K were easily achieved. A 10% CH_4/H_2 mixture at 1000 K would have an average translational energy for methane in excess of 30 kcal/mole, i.e., even greater than the calculated barrier height for CH_4 dissociative adsorption on W(110) **(8)**. Of course, a TOF spectrum of the CH_4 beam must be obtained to establish this claim.

B. Study of CD_4 at Low Surface Temperature

Gomer has observed **(31)** that for the activated diffusion of H adatoms and D adatoms on W(110), the transition from a tunneling to a thermally activated mechanism of diffusion is abrupt for H adatoms, but more gradual for D adatoms. An assessment of the importance of quantum tunneling in the dissociative adsorption of CH_4 on the Ir(110)-(1x2) surface may be obtained by a comparison of the behavior of CD_4 with respect to CH_4, when the surface is cooled.

V. CONCLUSIONS

A study of the role of translational energy in the dissociative adsorption of CH_4 on the Ir(110)-(1x2) surface has been reported. This work addresses the important area of C-H bond activation in the dynamics of alkane interaction with catalytic transition metal surfaces. From the results obtained, a lower limit of 13 kcal/mole has been calculated for the height of the barrier to

dissociative adsorption of CH_4 on the reconstructed Ir(110)-(1x2) surface. The dissociation probability associated with an average translational energy of methane equal to approximately 10 kcal/mole, has been determined experimentally to be less than 2×10^{-4}. Continued effort in the direction of the work presented in this chapter will contribute greatly to the understanding of gas-surface interactions.

Table 1.
Studies of the Interaction of CH_4 with Transition Metal Surfaces in UHV

Surface	T_s	Technique	Observations	$E_{dissociation\ barrier}$ (kcal/mole)	Ref.
Ni(111),(110) and (110)	300K	LEED, $\Delta\varphi$	$\Delta\varphi$ < leu in all cases but (111) < (110) < (100)		27
W(100)	300K 77K	H_2 TPD, $\Delta\varphi$	no evidence of dissociation but molecular adsorption at T_s = 77K		9
Rh, field emission tip	245K	H_2 TPD, $\Delta\varphi$, effusive molecular beam	increased $\Delta\varphi$ associated with heated CH_4 beam source	7	11
W, filament	600K→ 2600K	ΔPCH_4 using quadrupole mass spectrometer	$S \sim 3 \times 10^{-4}$ at T_s = 600K $S \sim 3 \times 10^{-5}$ at T_s = 2600K	2.7 at T_s = 600K 10.2 at T_s = 2600K	12 13
W, field emission tip	78K→ 2000K	$\Delta\varphi$, Field Emission Microscopy	for T_s = 70-800K, $S_0^{CH_4}$ decreases with increasing T_s above T_s = 800K S^{CH_4} increases with T_s at $T_s \sim$ 1000K, carbide structures observed		32
Ni(110)	298K→ 700K	AES,LEED Elipsometry	formation of nickel carbide at T_s = 473K to 579K, above T_s = 600K, C diffuses into the bulk		28
W(100), (111)	300→ 1000K	$\Delta\varphi$, Field Emission Microscopy	$\Delta\varphi < 0$ for $\theta_{carbon} \leq .2$ monolayer on W(100), $\Delta\varphi > 0$ for all θ on W(111)		33
Rh(111)	240K	Laser excitation of CH_4 (gas), H_2 TPD	no measurable CH_4 dissociation		10
Ir(110)-(1x2)	100K	TPD	no measurable adsorption		7
W(110)	800K	Molecular beams of CH_4 seeded in H_2,Ar, He and heated CO TPD	$S_0 = 4 \times 10^{-6}$ for $E_N^{CH_4}$ = 2.4 kcal/mole $S_0 = 2 \times 10^{-1}$ for $E_N^{CH_4}$ = 24 kcal/mole	25 kcal/mole	8
Ir(110)-(1x2)	700K	Molecular beams of CH_4 seeded in H_2, and He, CO TPD	dissociation probability of $CH_4 \leq 2 \times 10^{-4}$ for $E_N^{CH_4}$ = 10 kcal/mole	≥ 13 kcal/mole	

Symbols

LEED = low-energy electron diffraction

$\Delta\varphi$ = change in work function

TPD = temperature programmed desorption

ΔP = change in pressure

AES = Auger electron spectroscopy

S_0 = initial probability of adsorption

T_s = surface temperature

θ = fractional surface coverage

E_N = normal component of average translational energy

Table 2.
Average Translational Energy of CH_4 in Seeded Beams at 300 K

% CH_4 / Carrier Gas	V_c^{Pure} (cm/sec)	$\bar{\gamma}^{(a)}$	$\bar{m}$	$V_{CH_4}^{Mix}$ (cm/sec)	$\bar{E}_{CH_4}$ (kcal/mole)
1% CH_4/He	1.8×10^5	1.7	4.1	1.8×10^5	6.2
11% CH_4/H_2	3.0×10^5	1.4	3.5	2.3×10^5	10.2
1% CH_4/H_2	3.0×10^5	1.4	2.1	2.9×10^5	16.1
100% CH_4	1.2×10^5	1.3	16	-	2.8

(a) G. M. Barrow, 'Physical Chemistry', 3rd Ed., McGraw-Hill, NY, 1973.

REFERENCES

1. For a review of recent homogeneous transition metal catalyst work,see R. G. Bergman, Science **223**, 902 (1984).

2. For a review of metal cluster work, see E. L. Muetterties, Science **196**, 839, (1977).

3. For a recent review of heterogenous transition metal catalysts, studied in UHV, see W. H. Weinberg, Survey of Progress in Chemistry **10**, 1 (1983).

4. A. H. Janowisz and R. G. Bergman, J. Am. Chem. Soc. **104**, 352 (1982); **105**, 3929 (1983).

5. R. A. Periana and R. G. Bergman, in preparation.

6. W. D. Jones and F. J. Feher, Organomet. **2**, 562 (1983).

7. T. S. Wittrig, P. D. Szuromi and W. H. Weinberg, J. Chem. Phys. **76**, 3305 (1982).

8. C. T. Rettner, H. E. Pfnur and D. J. Auerbach, IBM, Surface Science, RJ 4505 (48513), 1984.

9. J. T. Yates Jr., and T. E. Madey, Surface Sci. **28**, 437 (1971).

10. J. T. Yates, Jr., J. J. Zinck, S. Sheard and W. H. Weinberg, J. Chem. Phys. **70**, 2266 (1979).

11. C. N. Stewart and G. Ehrlich, J. Chem. Phys. **62**, 4672 (1975).

12. H. F. Winters, J. Chem. Phys. **62**, 2454 (1975).

13. H. F. Winters, J. Chem. Phys. **64**, 3495 (1976).

14. K. Christmann and G. Ertl, Z. Naturforsch **28a**, 1144 (1973).

15. C.-M. Chan, M. A. Van Hove, E. D. Williams and W. H. Weinberg, Solid State

Commun. **29**, 47 (1979).

16. T. S. Wittrig and W. H. Weinberg, J. Chem. Phys. **72**, 4885 (1980).

17. In our laboratory the following procedure is used. The crystal is mounted on a goniometer [see J. F. Wendelken et al., Rev. Sci. Instrum. **48**, 1215 (1977), for a description of the goniometer], and oriented to ± 0.5° of the (110) plane, as determined by the Laue method (see, for example, E. Preuss, B. Krahl-Urban and R. Butz, "Laue Atlas", John Wiley and Sons, NY, 1974.). The crystal is mechanically polished on a Buehler (Buehler Apparatus for Microstructural Analysis, 41 Waukegan Road, Lake Bluff, IL, 60044) Handimet Grinder, using in succession, Buehler 240, 320, 400 and 600 abrasive paper. The crystal is then polished on a Bueler surfacer, using Metadi diamond pastes of 30, 6, 1 and 0.25 grit successively. The paste is applied to a clean polishing cloth mounted on the surfacer, and polishing at a particular grit size is continued until no scratches on the order of the grit size can be distinguished on the surface.

18. See, for example, P. W. Palmberg, G. E. Riach, R. E. Weber and N. C. Macdonald, "Handbook of Auger Electron Spectroscopy", Physical Electronics Industries, Inc., MI, 1972.

19. See, for example, R. B. Bernstein, "Chemical Dynamics via Molecular Beam and Laser Techniques", Oxford University Press, NY, 1982.

20. R. Sparks, private communication.

21. J. Cowin, private communication.

22. J. J. Zinck, C. B. Mullins and W. H. Weinberg, unpublished results.

23. J. L. Taylor, D. E. Ibbotson and W. H. Weinberg, J. Chem. Phys. **69**, 4298 (1978).

24. D. E. Ibbotson, T. S. Wittrig and W. H. Weinberg, J. Chem. Phys. **72**, 4885 (1980).

25. R. DiFoggio and R. Gomer, Phys. Rev. B **25**, 3490 (1982).

26. D. Schwarzkopf and R. Kieffer, Refractory Hard Metals, The Macmillan Co., NY. 1953.

27. G. Maire, J. R. Anderson and B. B. Johnson, Proc. Roy. Soc. (London)A **320**, 227 (1970).

28. F. C. Schouten, E. M. Kaleveld and G. A. Bootsma, Surface Sci. **63**, 460 (1977).

29. Thermocoax is manufactured by Amperax, Hicksville, L. I., N. Y., 11802.

30. G. Kruppa, private communication.

31. R. Gomer, Comments on Solid State Physics **10**, 253 (1983).

32. R. A. Shigeishi, Surface Sci. **51**, 377 (1975).

33. R. A. Shigeishi, Surface Sci. **72**, 61 (1978).

Figure Captions:

Fig. 1. Schematic view of the Ir(110)-(1x2) surface. Cross-hatched circles represent top-layer atoms, open circles represent second-layer atoms, and dotted circles represent third layer atoms. The scale of the methane molecule, using covalent radii for Ir, C, and H of 1.3 Å, 0.77 Å, and 0.32 Å, respectively, is shown also.

Fig. 2. AES spectra of the Ir crystal during sample cleaning. In each spectrum the vertical line indicates 256 eV on the horizontal axis. (For a reference to AES peak assignments see P. W. Palmberg, G. E. Riach, R. E. Weber and N. C. Macdonald, 'Handbook of Auger Electron Spectoscopy', Physical Electronics Industries Inc., MI, 1972.) A) a = 262 eV, C. B) a = 18 eV, Ir; b = 50 eV, Ir; c = 269 eV, C. C) a = 24 eV, Ir; b = 50 eV, Ir; c = 161 eV, Ir; d = 169 eV, Ir; e = 226 eV, Ir.

Fig. 3. Cross-sectional view of level II of the ultrahigh vacuum- molecular beam apparatus. a) Quartz nozzle. b) Skimmer. c) Collimating aperture mount; beam chamber 2→3. d) Collimating aperture mount; beam chamber 3→UHV. e) Gate valve; modified Huntington, pneumatic. f) Sample holder. g) Quadrupole mass spectrometer detector. h) Laser; He/Ne, alignment. i) Viewport. j) Vacuum coupling; beam chamber 1→oil diffusion pump. k) Low-energy electron diffraction port. l) Nozzle manipulator port.

Fig. 4. Thermal desorption spectra of CO after exposure of the clean Ir(110)-(1x2) surface to; a) 20 L molecular CO, b) 20 L C_2H_4 followed by thermal cycling of the crystal to 700 K to desorb H, and then exposure of the surface to 20 L of O_2. Arrows identify the maxima of thermal desorption features associated with a) and b).

Fig. 5. Schematice procedure of the experiment. a) Start beam running with beam isolation valve closed. b) Clean crystal. c) Stabilize crystal temperature at 700 K. d) Open beam isolation valve and expose crystal to the beam. e) Close beam isolation valve and cool crystal to 400 K. f) Expose crystal to 20 L of O_2. g) Flash crystal to 1200 K and record CO TPD. h) Flash crystal to 1600 K to remove any residual O from the surface.

Fig. 6. The results of the experiments detailed in Chapter 4. The number of C atoms on the surface after exposure to the beam is estimated from the CO TPD area. The number of CH_4 molecules from the beam which strike the surface is calculated from the measurement of the effective pressure of the beam (as described in Chapter 3 of this thesis) and from an estimation of the beam cross-sectional area explained in Chapter 4 of this thesis.

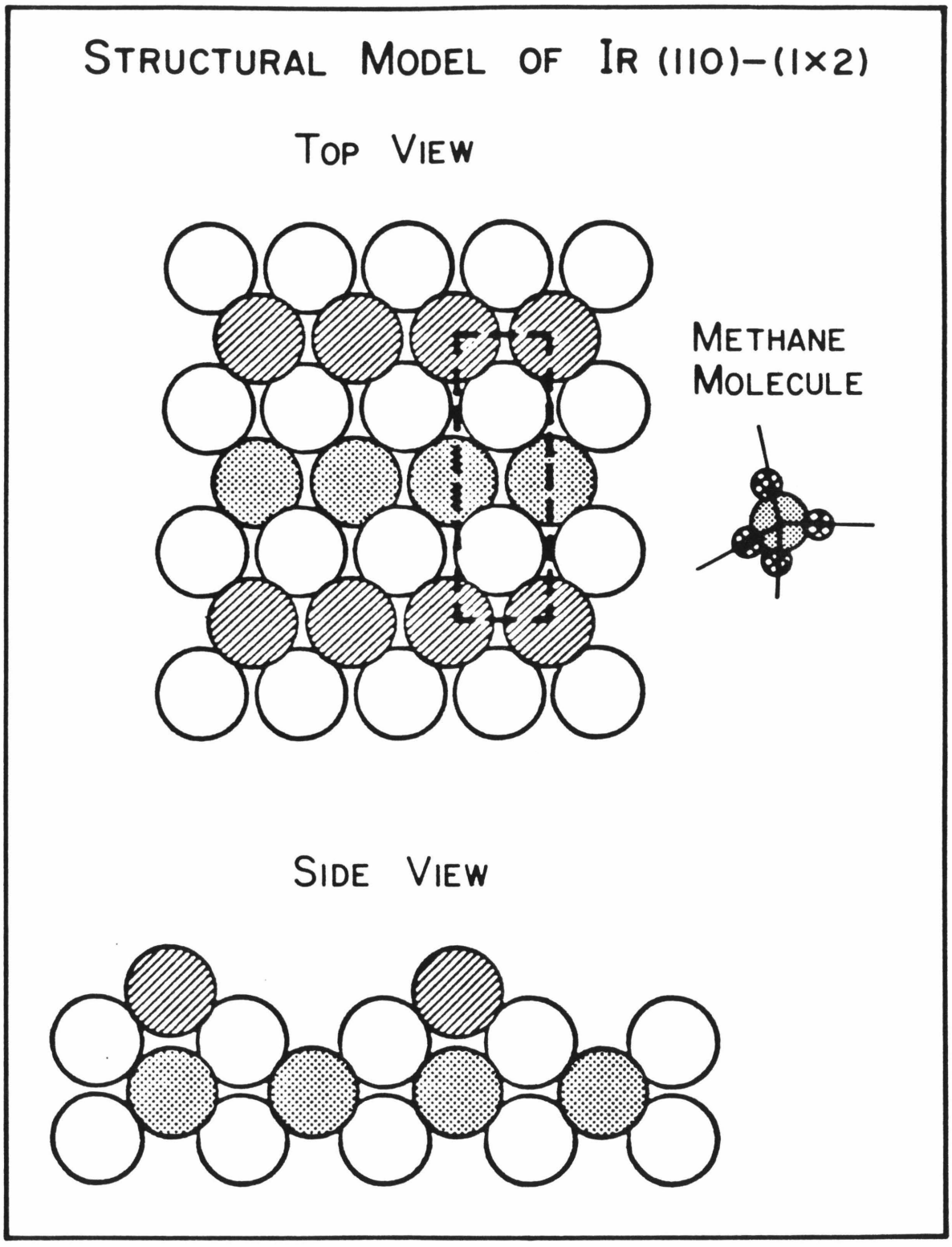
STRUCTURAL MODEL OF IR (110)-(1×2)
TOP VIEW
METHANE MOLECULE
SIDE VIEW

Fig. 1

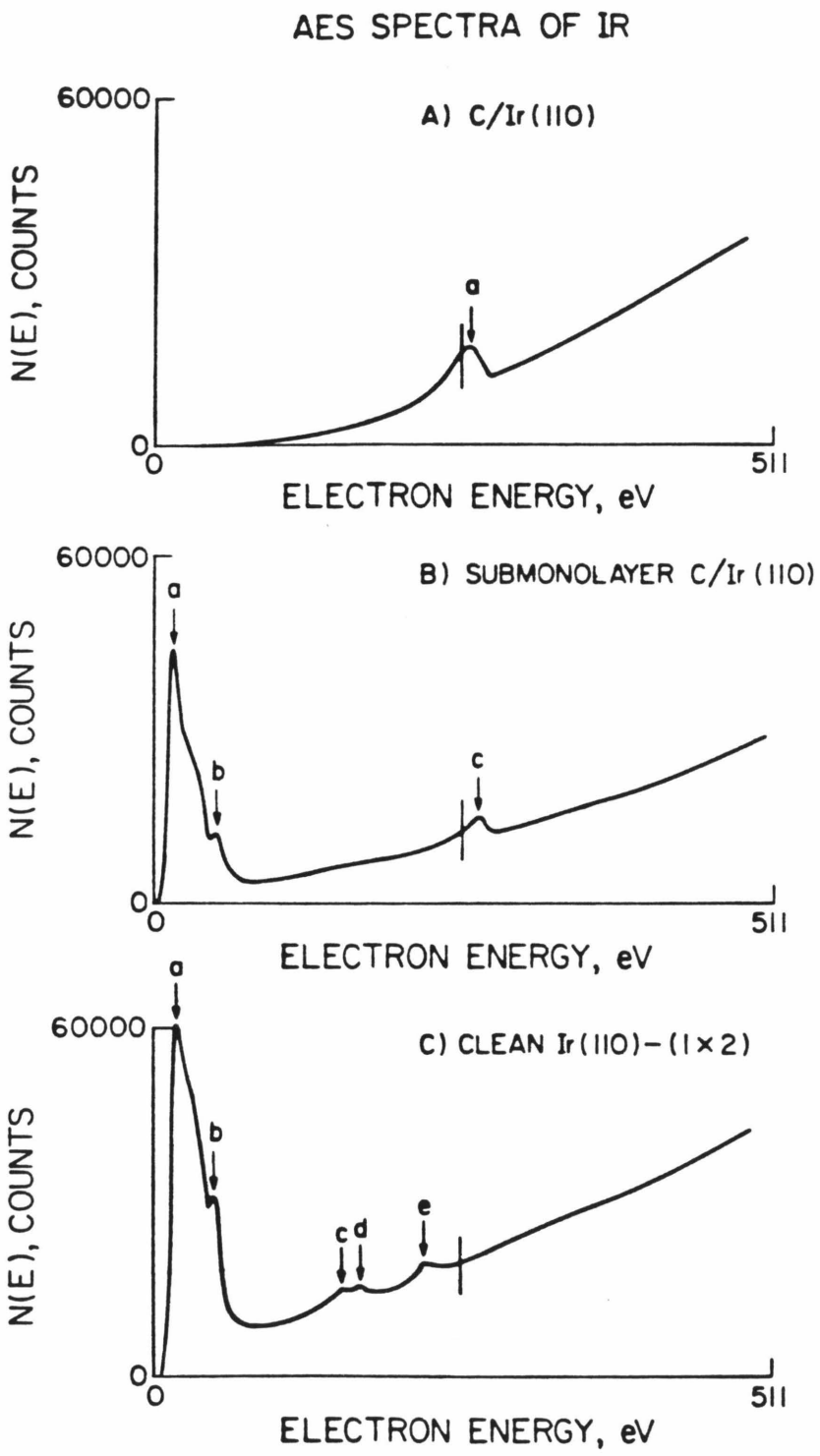
AES SPECTRA OF IR
60000
A) C/Ir(110)
N(E), COUNTS
a
0
0
511
ELECTRON ENERGY, eV
60000
B) SUBMONOLAYER C/Ir (110)
a
b
c
N(E), COUNTS
0
0
511
ELECTRON ENERGY, eV
a
60000
C) CLEAN Ir(110)-(1×2)
b
c d
e
N(E), COUNTS
0
0
511
ELECTRON ENERGY, eV

Fig. 2

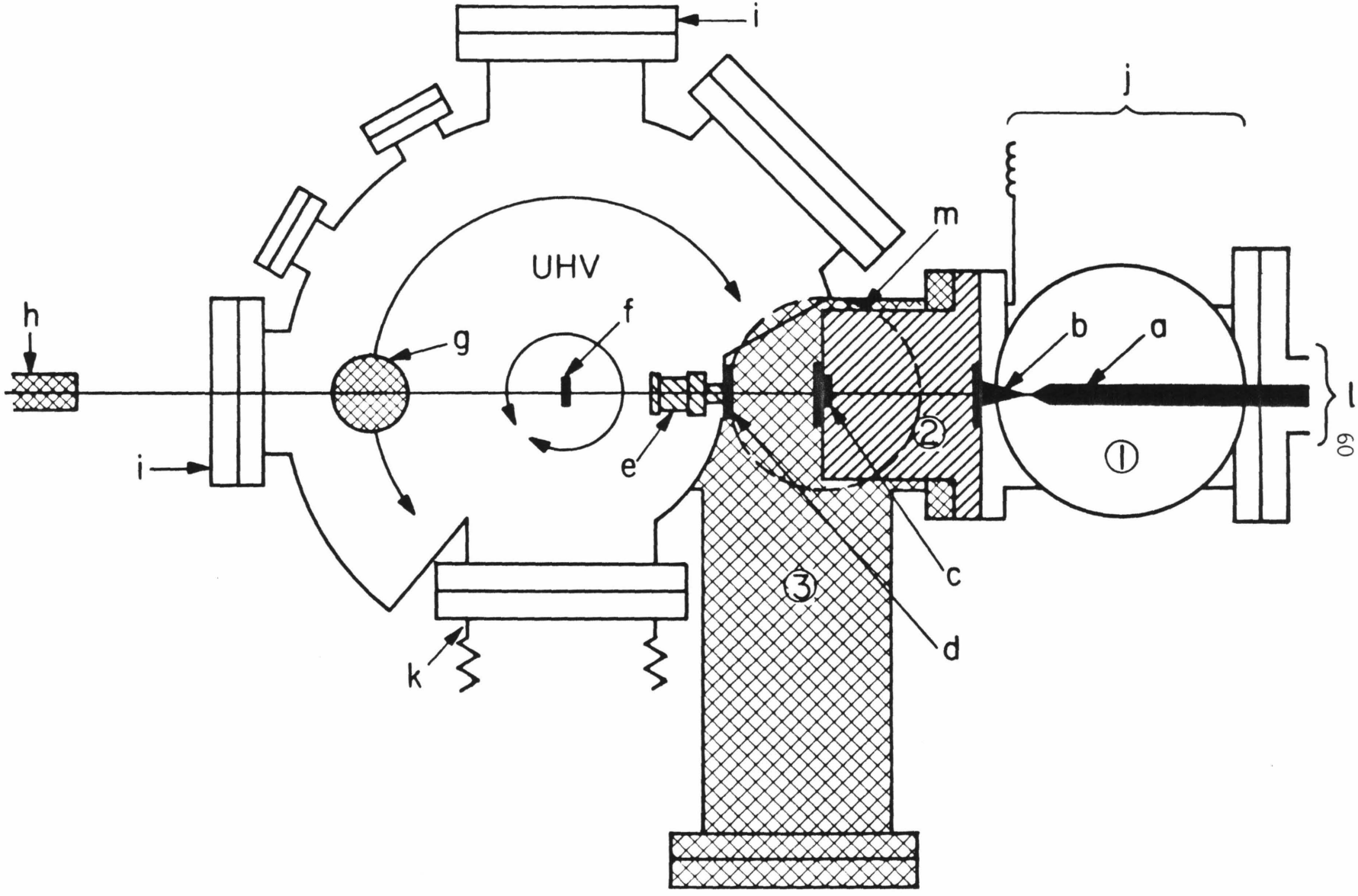

Fig. 3

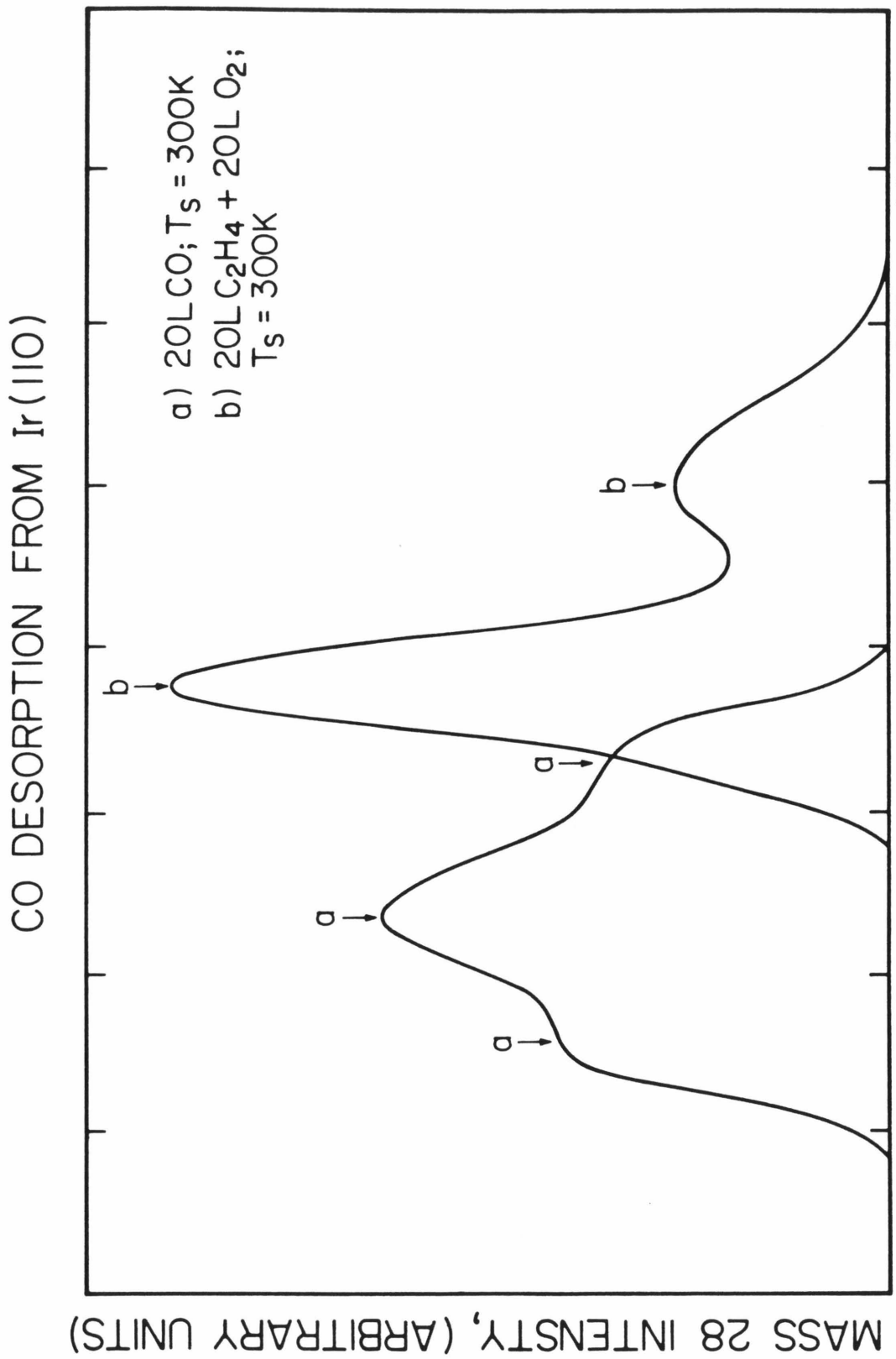
CO DESORPTION FROM Ir(110)
a) 20L CO; T_S = 300K
b) 20L C_2H_4 + 20L O_2; T_S = 300K
a
a
a
b
b
400
500
600
700
800
900
1000
TEMPERATURE, K
MASS 28 INTENSITY, (ARBITRARY UNITS)

Fig. 4

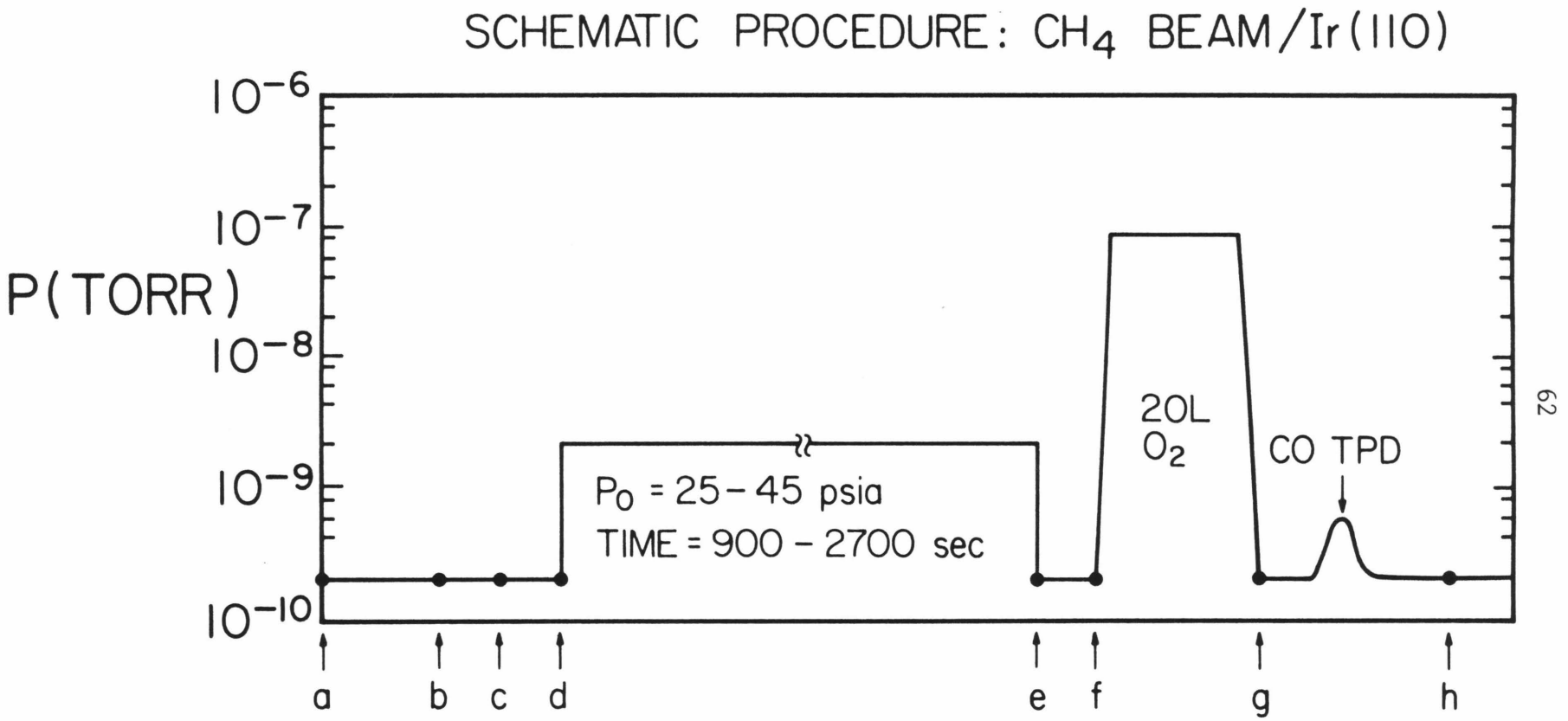
SCHEMATIC PROCEDURE: CH_4 BEAM/Ir(110)
P(TORR)
10^{-6}
10^{-7}
10^{-8}
10^{-9}
10^{-10}
P_0 = 25 - 45 psia
TIME = 900 - 2700 sec
20L
O_2
CO TPD
a
b
c
d
e
f
g
h

Fig. 5

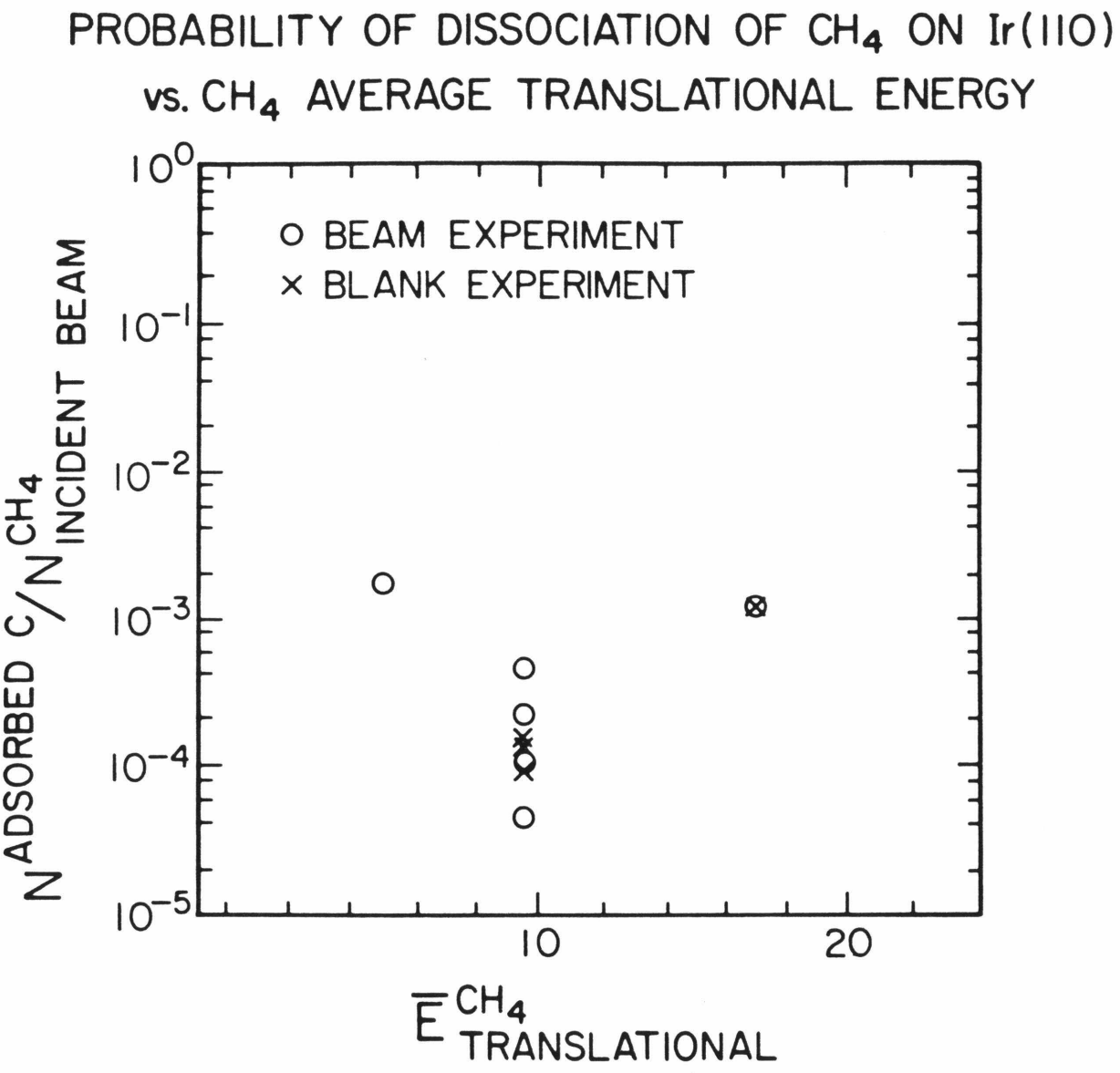
PROBABILITY OF DISSOCIATION OF CH_4 ON Ir(110)
vs. CH_4 AVERAGE TRANSLATIONAL ENERGY
10^0
10^{-1}
10^{-2}
10^{-3}
10^{-4}
10^{-5}
O BEAM EXPERIMENT
× BLANK EXPERIMENT
$N^{ADSORBED}_{INCIDENT\ BEAM}\ C/N^{CH_4}$
10
20
$\overline{E}^{CH_4}_{TRANSLATIONAL}$

Fig. 6

APPENDIX A

SUMMARY ABSTRACT: CHEMISORPTION OF WATER ON Rh(111)

[The text of Appendix A consists of an article coauthored with W. H. Weinberg which has appeared in *The Journal of Vacuum Science and Technology* **17**, 188 (1980).]

Summary Abstract: Chemisorption of water on Rh(111)

J. J. Zinck[a] and W. H. Weinberg[b]

Division of Chemistry and Chemical Engineering, California Institute of Technology, Pasadena, California 91125

(Received 4 September 1978; accepted 5 November 1979)

PACS numbers: 68.45.Da, 82.65.My

The chemisorption of H_2O on the (111) surface of Rh has been studied by thermal desorption mass spectrometry and low-energy electron diffraction. In addition to the clean surface, the chemisorptive behavior of H_2O has been examined when various coverages of oxygen, hydrogen, or carbon monoxide have been pre-adsorbed on the surface in the form of atomic oxygen, atomic hydrogen and molecular CO.

At coverages of less than 10% of saturation on the clean surface, only one feature appears in the thermal desorption spectra of H_2O, with a peak temperature of approximately 191 K. This feature is attributed to the weakly chemisorbed first monolayer of water on the surface. As the coverage is increased, a broadening of the first monolayer feature is observed and a low temperature shoulder appears in the thermal desorption spectra which develops into a second feature with a peak temperature of approximately 165 K. This second feature, observed near 70% of saturation of the first monolayer, corresponds to the formation of multilayers of H_2O on the Rh(111) surface.

The adsorption kinetics of the first monolayer of H_2O on the clean Rh(111) surface are shown in Fig. 1. The data indicate a dependence of coverage on exposure which appears approximately linear suggesting a mobile precursor model of adsorption. The constant sticking probability of $S_0 = 0.58$ is calculated from a least squares fit to the data weighted by the standard deviation in the coverage values. In addition, theoretical results for first-, second- and half-order Langmuir adsorption kinetics are presented in Fig. 1. Clearly, the adsorption of water on Rh(111) does not correspond to first- or second-order Langmuir kinetics. However, it would be incorrect to preclude half-order adsorption kinetics entirely in favor of the precursor model. It is possible that half-order adsorption kinetics corresponds to the formation of islands of H_2O on the surface. The formation of islands of H_2O may also explain why the multilayer feature appears in the thermal desorption spectra before the first monolayer is completely saturated. A conclusive assignment of the adsorption kinetics cannot be made on the basis of these data alone.

Using the method of Chan *et al.*,[1] the activation energy of desorption of H_2O from the clean surface was calculated as 17 kcal/mol with an unusually high pre-exponential factor of $9.2 \times 10^{19}\ s^{-1}$ in the limit of zero coverage. Alternatively, assuming a pre-exponential factor of $10^{13}\ s^{-1}$ fixes the energy of desorption at 7.5 kcal/mol. This value seems unreasonably low with respect to the heat of sublimation of normal ice, 12.1 kcal/mol, corresponding to the desorption energy of the multilayer from the surface. Further experiments to measure isosteres are proposed to attempt to clarify the desorption kinetics.

A $(\sqrt{3} \times \sqrt{3})R30°$ LEED pattern is observed for the first monolayer of H_2O on the surface. After saturation of the first monolayer, additional exposure of the surface to H_2O causes formation of multilayers of H_2O which obscure the LEED pattern. This observation indicates that the multilayer itself is not ordered.

Three different oxygen overlayers were prepared on the Rh(111) surface to act as substrates for the chemisorption of H_2O. An ordered $[(2 \times 2)]$ unsaturated oxygen overlayer corresponding to approximately 30% of saturation, a saturated unordered oxygen overlayer and a saturated ordered $[2 \times 2)]$ oxygen overlayer were all prepared using results of a previous investigation of the chemisorption of O_2 on Rh(111).[2]

Three features are observed in the thermal desorption spectra of H_2O from each oxygen covered Rh(111) surface which differ in their rates of saturation, but not in peak temperature, from surface to surface. At the lowest exposures, a peak near 220 K is observed for all three oxygen covered Rh surfaces which may result from hydrogen bonding of water to surface oxygen. A second feature, with peak temperature near that of the first monolayer on the clean surface, begins to appear after an exposure of 1.1 L (1 L = 1 Langmuir = 10^{-6} Torr s) on the unsaturated ordered oxygen/Rh(111) surface, an exposure of 0.44 L on the saturated unordered oxygen/Rh(111) surface, and is already present at the lowest exposure of 0.22 L on the saturated ordered oxygen/Rh(111) surface.

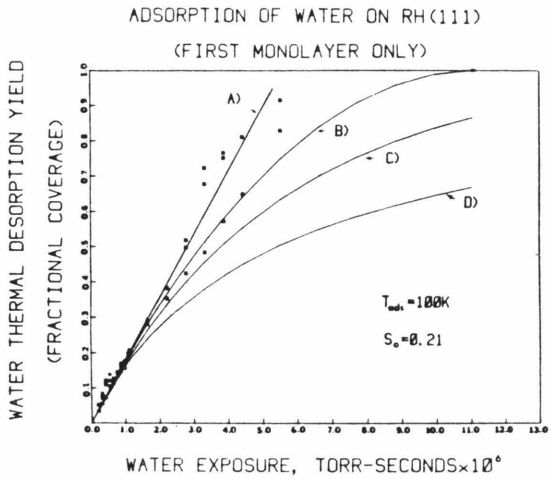

FIG. 1. Adsorption kinetics of the first monolayer of H_2O on the clean Rh(111) surface: (a) Least squares fit to the data weighted by the standard deviation in the coverage values; (b) Theoretical plot of half-order Langmuir adsorption kinetics, $S_o = 0.58$; (c) Theoretical plot of first-order Langmuir adsorption kinetics, $S_o = 0.58$; (d) Theoretical plot of second-order Langmuir adsorption kinetics, $S_o = 0.58$.

 0022-5355/80/010188-02$01.00

The third feature, identified as desorption of the multilayer, appears at an exposure of 3.33, 1.5, and 0.8 L on the unsaturated ordered oxygen/Rh(111), saturated unordered oxygen/Rh(111) and saturated ordered oxygen/Rh(111) surfaces, respectively. The multilayer initially appears at a peak temperature almost 10 K higher than the clean surface for all the oxygen/Rh(111) surface, suggesting that low concentrations of multilayer on the surface are still influenced by surface oxygen. The peak temperature of the multilayer drops rapidly to the clean surface value as the amount of multilayer on the surface is increased past several monolayers.

An unsaturated hydrogen overlayer, corresponding to approximately 40% of saturation, and a saturated hydrogen overlayer were prepared as described previously[3] and were used as substrates for the chemisorption of H_2O.

The thermal desorption spectra of H_2O from the unsaturated hydrogen/Rh(111) surface resemble those obtained on the clean surface with respect to features observed and peak temperatures. A saturation coverage of hydrogen on Rh(111) essentially prohibits formation of any feature but the multilayer. However, a small high temperature shoulder is observed, suggesting the presence of a small amount of weakly chemisorbed H_2O. The multilayer peak temperature corresponds to that found on the clean surface. It appears that although the presence of oxygen on the surface distinctly affects the chemisorption of H_2O, no such effect is observed due to the presence of hydrogen on the surface.

An unsaturated CO overlayer, corresponding to a coverage of 45% of saturation and chosen to produce the maximum intensity in the $(\sqrt{3} \times \sqrt{3})R30°$ CO LEED pattern as reported previously and corresponding to 1/3 monolayer,[4] and a saturation coverage of CO on Rh(111) were also prepared and used as substrates for the chemisorption of H_2O.

As in the case of unsaturated hydrogen/Rh(111), the thermal desorption spectra of H_2O from the unsaturated CO/Rh(111) surface closely resemble those of the clean surface in spectral features and peak temperatures. Only the multilayer feature accompanied by a small high temperature shoulder is observed in the thermal desorption spectra of H_2O from a saturated CO/Rh(111) surface. A saturation coverage of CO blocks almost all the chemisorption of H_2O as observed with the saturated hydrogen/Rh(111) surface.

ACKNOWLEDGMENT

This work supported by the National Science Foundation under Grant No. DMR77-149 76

[a]National Research Council of Canada Predoctoral Fellow.
[b]Camille and Henry Dreyfus Foundation Teacher-Scholar.

[1]C.-M. Chan, R. Aris and W. H. Weinberg, Appl. Surf. Sci. **1**, 360 (1978).
[2]P. A. Thiel, J. T. Yates, Jr., and W. H. Weinberg, Surf. Sci. **82**, 22 (1979).
[3]J. T. Yates, Jr., P. A. Thiel, and W. H. Weinberg, Surf. Sci. **84**, 427 (1979).
[4]P. A. Thiel, E. D. Williams, Y. T. Yates, Jr., and W. H. Weinberg, Surf. Sci. **84**, 54 (1979).

APPENDIX B

EXTENDED TRAVEL ULTRAHIGH VACUUM SAMPLE MANIPULATOR WITH TWO ORTHOGONAL, INDEPENDENT ROTATIONS

(The text of Appendix B consists of an article coauthored with W. H. Weinberg which is to appear in the *Review of Scientific Instruments*).

Ideally, an ultrahigh vacuum (UHV) compatible sample manipulator should allow all degrees of rotational and translational freedom of the sample, independently, and without inducing strain on any part of the manipulator, provide heating and cooling for the sample, and be easily demountable from the UHV chamber. In practice, it is often difficult to satisfy all these conditions, and some aspects of design are favored preferentially, according to the needs of a particular experiment **(1-5)**.

We have designed a manipulator compatible with our ultrahigh vacuum molecular beam apparatus **(6)** which has the following features: resistive heating and liquid nitrogen cooling of the sample, 1/2" of XY (horizontal) and 2" of Z (vertical) translation provided by a commercial (Huntington #PM-275-XYZ) precision translator, an additional 22" of Z translation via a separately supported welded bellows (Standard Bellows # 249-153-25-EE), a gimbals assembly which provides 1° of tilt for the manipulator shaft, and mechanisms for 360° of independent polar (θ) and azimuthal (φ) sample rotation. In addition, the sample holder is sufficiently compact to be withdrawn into a load lock of 1 1/2" inner diameter, which may be isolated from the UHV chamber by a gate valve of the same dimension.

The mechanism of polar rotation of the sample has been adapted from the design of Unwin et al. **(7)** and consists of two sliding seals of a type first described by Wilson **(8)**. In this design, a rotary shaft handle makes a seal against two viton gaskets mounted in an external housing. The interstitial space between the viton gaskets is pumped differentially by a mechanical pump to a pressure on the order of 50 microns. This differential pumping reduces the gas leakage into the UHV chamber to a negligible load when the rotary shaft handle is turned. A stainless steel tube, which acts as a cryostat for the sample and to which the sample holder is attached, makes a UHV seal

to the rotary shaft handle.

Our manipulator incorporates the same differential pumping arrangement as in the design of Unwin et al. **(7)**, but has the following modifications to the cryostat and sample holder. The main shaft of the cryostat is constructed from a 3/4" O.D. x 5/8" I.D. stainless steel tube that is 3' in length. A 1' length of 9/16" O.D. x 3/8" I.D. stainless steel tube is welded to one end of the main shaft. The smaller tube is then sealed to the rotary shaft handle via a series of knife edge seals as shown in Fig. 1. The outer diameter of the double knife edge ring, the small copper gasket and the spacer ring have been machined 0.010" smaller than the inner diameter of the rotary shaft handle to facilitate pumping of interstitial air. This arrangement provides us with a means of separating the manipulator shaft from the differential pumping housing, by allowing us to drop the shaft beneath the housing once the UHV seals have been broken. This offers the advantage that a conflat flange may be welded to the bottom of the cryostat,and any commercial feedthrough may be selected to provide the desired connections to the sample holder. We are currently using a single thermocouple (W/5%Re,W/26%Re) power feedthrough mounted on a miniconflat flange (Ceramaseal # 808BB8871-2). We have encountered no problems with respect to vacuum integrity of the copper conflat seal after extended and repeated exposure of the seal to liquid nitrogen.

The azimuthal rotation mechanism consists of an upper and lower assembly connected via a spring loaded Be-Cu wire. The lower assembly is subject to the restriction that the sample holder must pass through a 1 1/2" I.D. tube (6). As a consequence the assembly is very compact, as can be judged from the scale in Fig. 2(b).

In the upper assembly [Fig. 2(a)], a miniature bearing (MPB # S6316RHHE5P28LD) is press fit to a disk [the upper bearing housing of Fig. 2(a)]. A filister screw captures the inner race of the bearing and secures the disk to a bushing which is mounted on the manipulator shaft. A raceway is machined in the circumference of the disk for a Be-Cu 3/4 hard wire. The I.D. of the disk is threaded to receive a coupling which connects the upper assembly to a rotary motion feedthrough (Huntington #VF-106). The coupling is bored and slotted so that the shaft of the rotary motion feedthrough may be slip fit to the coupling I.D. A pin fixed on the feedthrough shaft lies in the slot of the coupling to effect the transfer of force which will move the assembly when the rotary motion feedthrough is turned. A lock nut on the feedthrough prevents the rotation of the azimuthal mechanism when the manipulator is moved in any of its other degrees of freedom.

The upper assembly is positioned on the cryostat shaft at the level of a vacuum fitting such that a port with a miniconflat flange is available for mounting the rotary motion feedthrough, which subsequently holds the upper assembly in place.

The lower assembly contains the same type of miniature bearing as the upper assembly. In this case, the miniature bearing is press fit to a stainless steel plate which supports the sample holder. The plate is fastened with three screws to a stainless steel split ring clamp mounted on the Ceramaseal feedthrough above the weld lip. A stainless steel spindle captures the inner race of the bearing. On one end of the spindle a raceway approximately 1/32" wide is machined, in which the Be-Cu wire travels. The ratio of the circumference of the lower to upper raceways is 1:2. Although the bearings of the upper and lower assembly are not lubricated, we have experienced no difficulty with seizing of the mechanism.

The sample holder consists of a Macor (9) disk and sample supports. The Macor disk is slip fit to the O. D. of the spindle on the end opposite the raceway and held in place by set screws. Tantalum heating wires of 0.010" diameter spotwelded to the back of the crystal are clamped to copper rods of 0.094" diameter mounted in the Macor disk and held in place by set screws. Flexible copper braid connectors 0.08" wide by 3" long provide the conduction path from the feedthrough to the crystal. Thermocouple wires 0.010" in diameter are anchored in the Macor disk via set screws.The crystal thermocouple of 0.003" diameter wire is spotwelded to the back of the crystal and spotwelded to the 0.010" diameter thermocouple wire mounted in the Macor. Thermocouple wire of 0.003" diameter is also connected from the feedthrough thermocouple posts to the 0.010" wire anchored in the Macor with sufficient slack to allow ± 180° of azimuthal rotation.

The upper and lower assemblies are connected by a #30 Be-Cu 3/4 hard wire which is loaded by two springs mounted approximately 3" below the upper assembly. The springs are constructed from #22 Be-Cu 3/4 hard wire. They have an O.D. of 0.23", are 2 1/2" long and contain 70 coils. After winding and before mounting, the springs are stress relieved by annealing them at 300°C for three hours. When mounted the springs are extended in length to 3 1/2" (approximately 70% of their maximum deflection), corresponding to a load of about 1 1/2 pounds.

Turning the rotary motion feedthrough turns the coupling and the upper bearing housing. Tension on the wire provided by the springs succeeds in transferring the force to the lower assembly and in turning the spindle and the Macor disk. Due to relaxation of the spring and wire with thermal cycling, such as bakeout of the vacuum chamber, and slippage of the wire in the raceways, angular displacements will not necessarily correlate with

displacement of the rotary motion feedthrough. In order to measure the relative change in azimuthal angle, a dial graded in degrees is mounted on the lower bearing housing which encircles the macor disk while leaving it free to rotate. A vernier is mounted on the Macor disk providing an angular resolution of approximately 0.2°. The dial may be read using a telescope or cathetometer. An absolute determination of the azimuthal angle may be obtained from low-energy electron diffraction, when optics are available.

We have been successfully employing this manipulator for one year in our UHV system, where the base pressure is typically less than 2×10^{-10} Torr after a 24-hour bakeout at 120°C.

This work was supported by the Army Research Office under Contract No. DAAG29-83-K-0094.

References

1. C. J. Russo and R. Kaplow, J. Vac. Sci. Technol. **13**, 487 (1976).

2. P. H. Citrin, P. Eisenberger and R. C. Hewitt, Phys. Rev. Lett. **45**, 1948 (1980).

3. K. D. Jamison and F. B. Dunning, Rev. Sci. Instrum. **55**, 1509 (1984).

4. P. A. Thiel and J. W. Anderegg, Rev. Sci. Instrum. **55**, 1669 (1984).

5. J. A. Strocio and W. Ho, Rev. Sci. Instrum. **55**, 1672 (1984).

6. J. J. Zinck and W. H. Weinberg, in preparation.

7. Von R. Unwin, K. Horn and P. Geng, Vakuum-Technik **29**, 149 (1980).

8. R. R. Wilson, Rev. Sci. Instrum. **12**, 91 (1941).

9. Macor is a machinable glass ceramic manufactured by Corning Glass Works, Corning NY 14831.

Figure Captions

Figure 1: Upper manipulator housing and shaft seals: (A) Cryostat tube. (B) Rotary shaft handle. (C) Differential pumping housing. (D) Viton gasket. (E) Miniconflat flange. (F) Copper gasket. (G) Double knife edge ring. (H) Knife edge machined on cryostat tube. (I) Spacer ring. (J) Split ring. (K) Miniconflat flange connection to mechanical pump.

Figure 2: *(a)* Upper assembly of azimuthal rotation mechanism: (A) Miniature bearing. (B) Upper bearing housing disk. (C) Fillister screw. (D) Bushing. (E) Raceway. (F) Be-Cu wire. (G) Coupling. (H) Rotary motion feedthrough. (I) Pin. (J) cryostat shaft (9/16" O.D.). (K) Cryostat shaft (3/4" O.D.). (L) Be-Cu spring. (M) Vacuum fitting.

(b) Lower assembly of azimuthal rotation mechanism and sample holder: (A) Miniature bearing. (B) Plate for lower bearing housing and sample holder support. (C) Split ring clamp. (D) Ceramaseal feedthrough. (E) Weld lip. (F) Spindle. (G) Raceway. (H) Macor disk. (I) Cu rod (0.094" dia.). (J) Flexible Cu braid. (K) Thermocouple wire (0.010" dia.). (L) Thermocouple wire (0.003" dia.). (M) Be-Cu wire. (N) Graded dial. (O) Vernier. (P) Feedthrough thermocouple post. (Q) Feedthrough heating/cooling rod. (R) Cryostat shaft. (S) Miniconflat flange copper gasket seal. (T) Cap screw. (U) Set screw. (V) Ta heating wire (0.010" dia.). (W) Crystal sample.

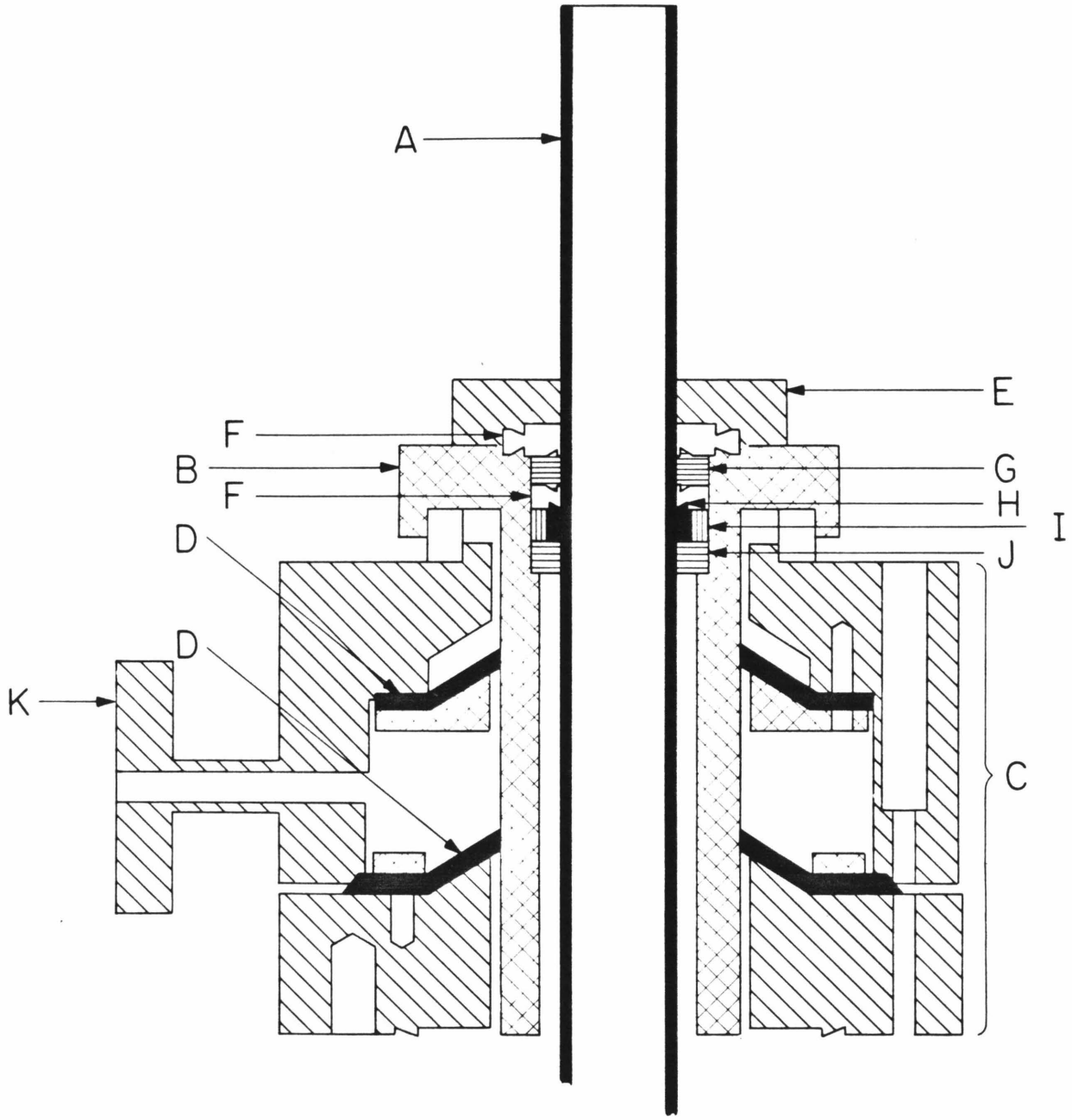

Fig. 1

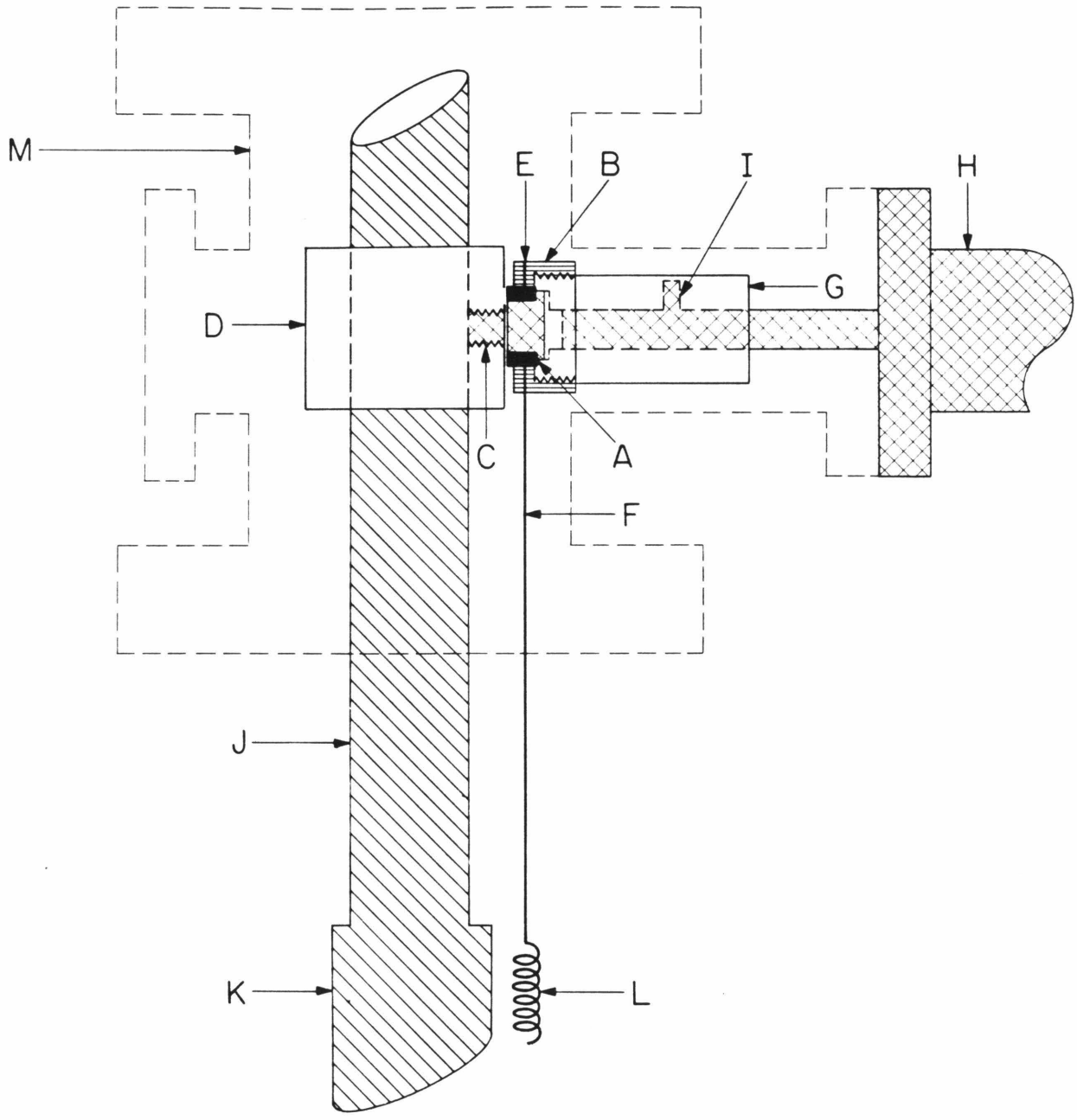

Fig. 2a

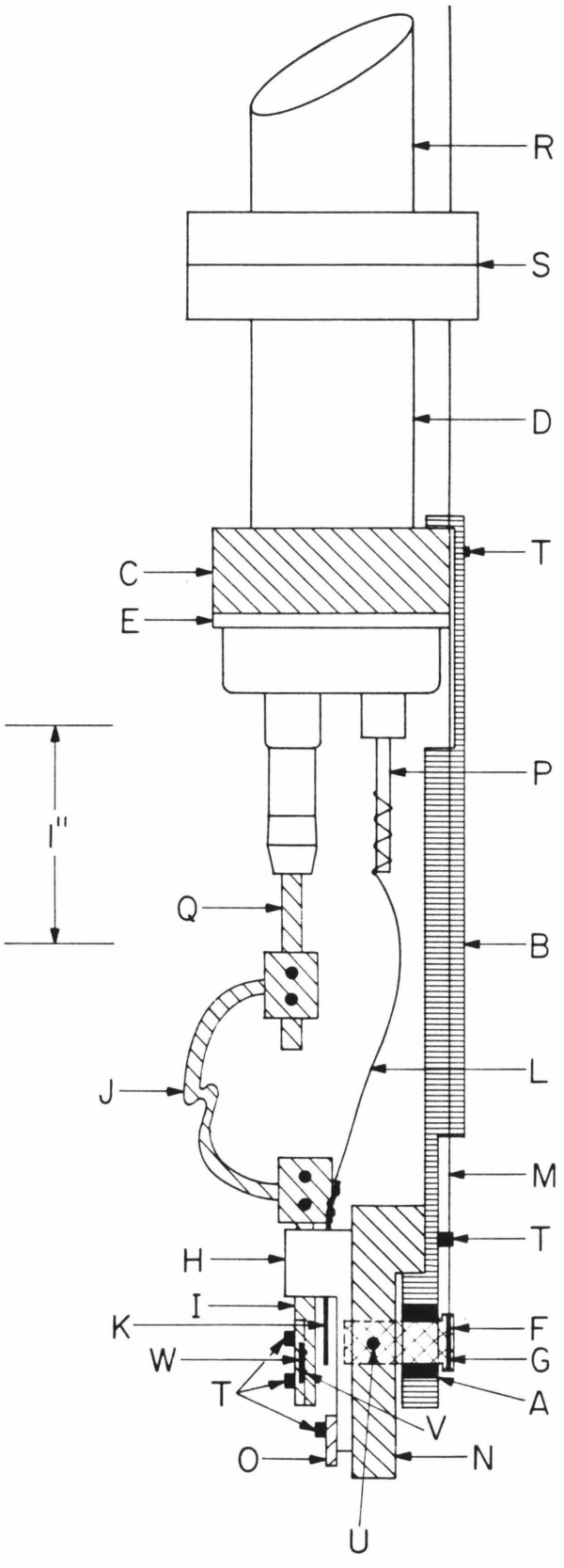

Fig. 2b

APPENDIX C

PNEUMATIC GATE VALVE MOUNTED INSIDE AN ULTRAHIGH VACUUM CHAMBER

[The text of Appendix C consists of an article coauthored with W. H. Weinberg which has appeared in the *Review of Scientific Instruments*) **55**, 810 (1984)].

We have modified a commercial pneumatic gate valve (Huntington # GVAP-062) so that both the gate and its actuating mechanism are ultrahigh vacuum (UHV) compatible. We are successfully using this modified valve to isolate our UHV chamber from a supersonic molecular beam line. Mounting the isolation valve inside the vacuum chamber has the advantage that the valve does not contribute to the source-to-sample path length. In addition, the valve may be interfaced to the system interlock since its operation is controlled by a solenoid valve.

In order to mount a pneumatic valve in UHV, it is necessary to compensate for gas leakage which occurs across the pistons of the mechanism and into the UHV chamber, as shown in Fig. 1a. This leakage occurs because the lower housing in which the pistons are mounted does not have a machined sealing surface, and because there is no vacuum seal between the lower housing and the central section of the valve. Simply placing a seal between the central section and the lower housing will not suffice, because pressure buildup above the floating piston may lead to an unreliable gate seal and undesirable stress on the valve bellows which is designed for a maximum 15 psi pressure differential.

Our modification involves enlarging the central section of the valve and machining the necessary O-ring grooves and sealing surfaces so that the central section can be pumped differentially, as shown in Fig. 1b. The vertical height of the new central section was increased to 1-1/2" in order to accommodate both the weld to the bellows and a 1/4" O.D. 304 stainless steel tube (1/32" wall thickness) welded into this section for a pumping port. We lengthened the center shaft by the difference in height of the new and old central sections and welded the new shaft into the upper end of the bellows. The original bellows was replaced with one of similar specifications (Standard

Bellows # 64-34-5-EE) **(1)**. An O-ring groove was machined in both the upper surface (Parker O-ring # 2-26) and the lower surface (Parker O-ring # 2-21) of the new central section.

The lower housing of the valve is constructed of aluminum and anodized black, with stainless steel fittings which are furnace brazed **(2)** to the aluminum for the connection of air lines. To insure UHV compatibility, the lower housing was separated from the rest of the valve and sandblasted to remove the pigment used in the anodization. Stainless steel tubes of 1/8" O.D. × 1/16" I.D. were welded into the air line fittings. The two air line fittings and the pumping port were welded to a 3-3/8" O.D. conflat flange and mated to an identical flange inside the UHV chamber.

The piston O-rings were greased with a low vapor pressure, high temperature lubricant (Apiezon T). The viton O-ring seals of the upper and lower surfaces of the central section were not greased. The assembled valve was mounted onto the appropriate mating flanges inside the UHV chamber via the mini conflat flange of the upper housing of the commercial gate valve and the 3-3/8" conflat flange into which the air lines and pumping port were welded. The central section of the valve was pumped by a 10 l/min^{-1} mechanical pump. The valve was operated with 55 psi of high purity nitrogen.

The UHV chamber, pumped by a 2000 l/s turbomolecular pump, was baked at 80°C for 24 hours, after which the base pressure was 1×10^{-10} Torr with the beam line at atmospheric pressure.

To summarize, we have demonstrated that the pneumatic actuating mechanism of a miniature gate valve can be made UHV compatible by the addition of a differential pumping section to compensate for gas leakage

across the pistons of the valve mechanism.

References

1. The same effective modification could also be made without replacing the original bellows. Rather than machining a new central section, a similar piece may be placed between the existing central section and the lower housing. This sector need only be sufficiently high to accommodate a pumping port tube of the desired size and be machined with O-ring grooves on its upper and lower faces. The center shaft may then be lengthened the appropriate amount by an extension piece which threads into the end of the existing shaft. The lower face of the existing central section must also be polished smooth for the O-ring seal.

2. American Welding Society. Committee on Brazing and Soldering *Brazing Manual*, Reinhold Publishing Corp. (1963), p. 133.

Figure Caption

Figure 1a: Cross sectional view of unmodified valve. (A) Gate assembly. (B) Bellows. (C) Center shaft. (D) Copper wire seal between upper housing and central section. (E) Floating Piston. (F) Gas inlet to open gate. (G) Fixed piston. (H) Gas inlet to close gate. (I) O-ring.

Figure 1b: Cross sectional view of modified valve. (A) Port to mechanical pump. (B) Gas lines. (C) Additional O-ring seals.

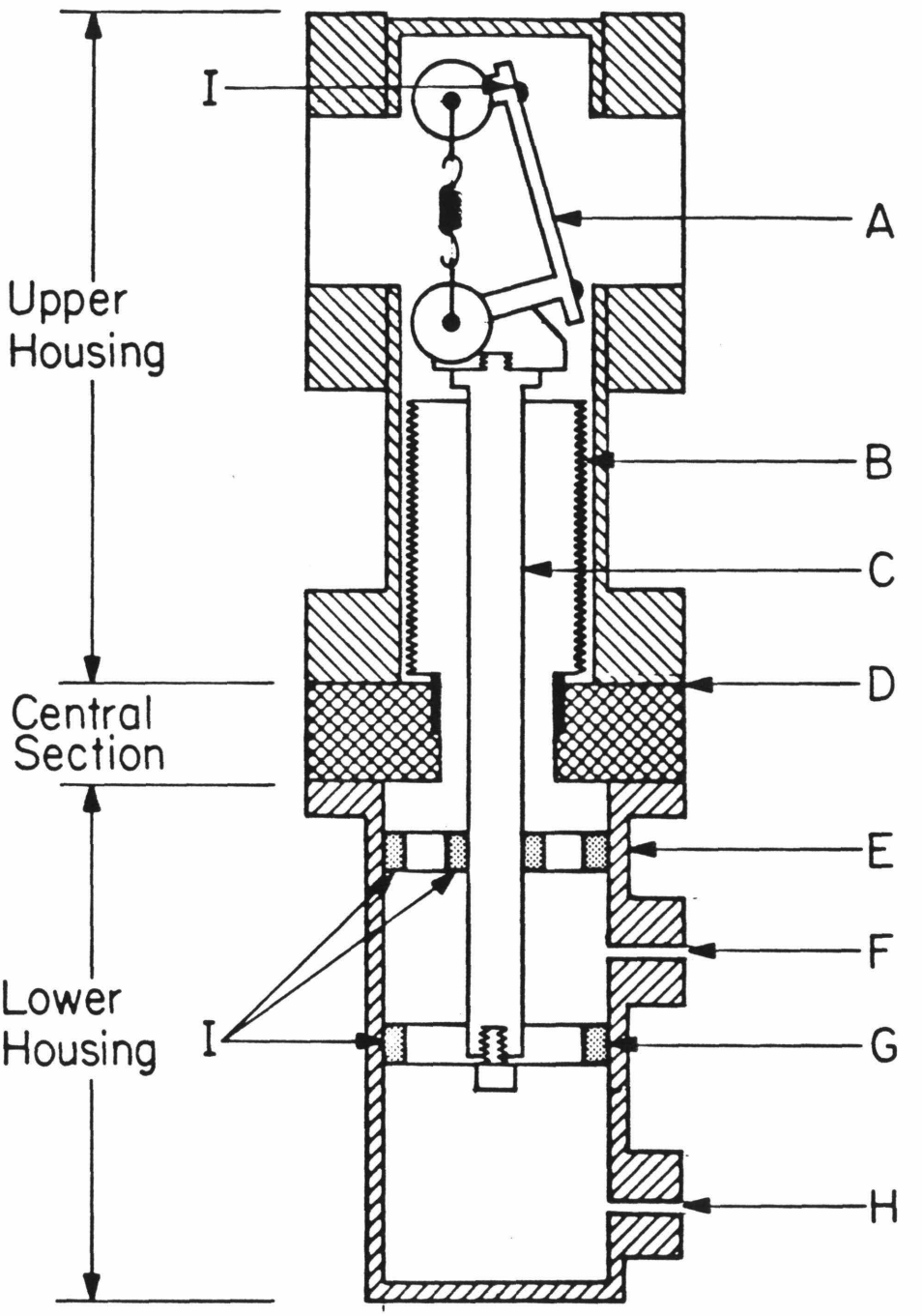

Fig. 1a

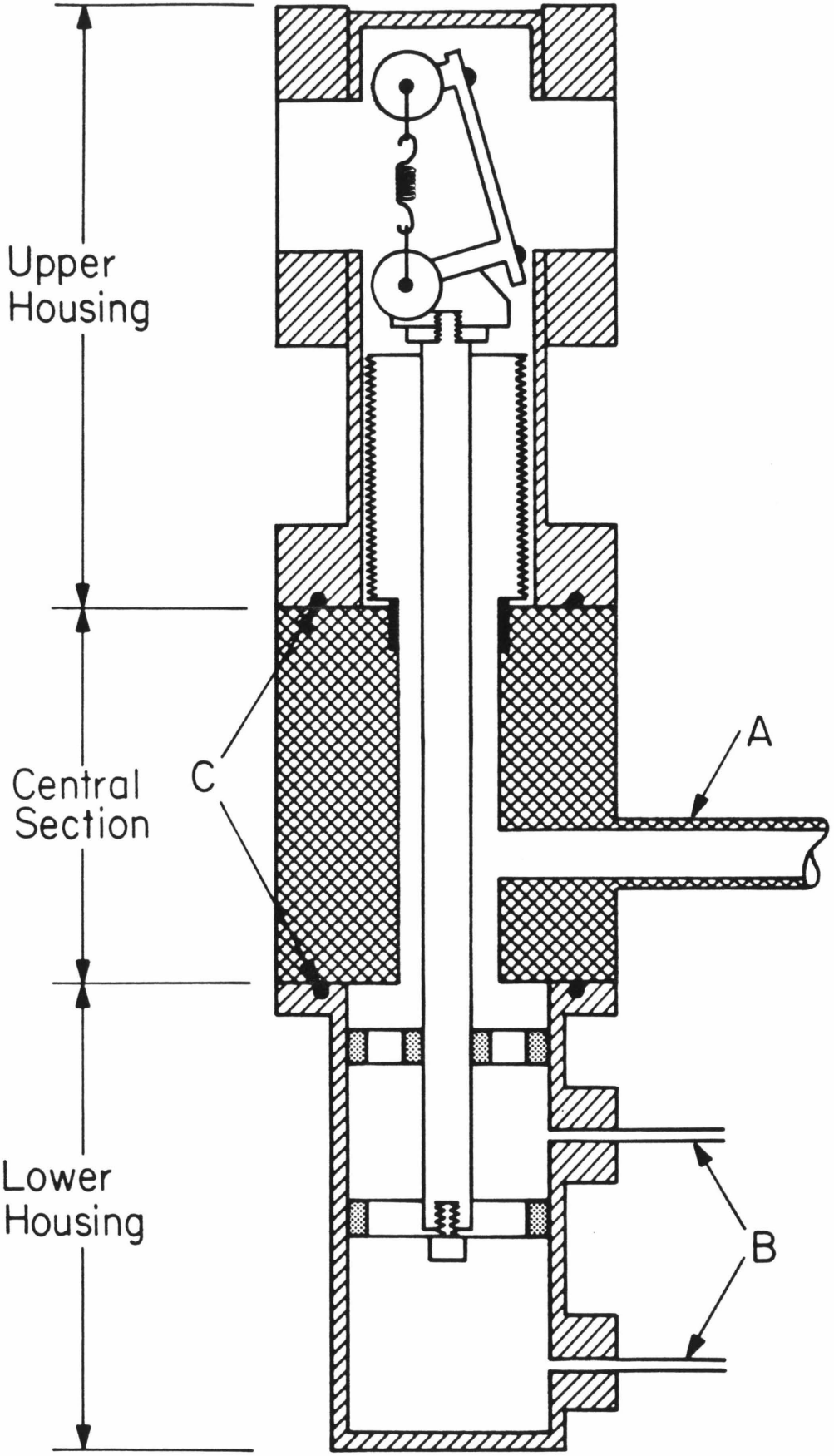

Fig. 1b

APPENDIX D

PREPARATION AND PURITY MEASUREMENT OF EXTREMELY PURE HELIUM GAS

[The text of Appendix D consists of an article coauthored with John T. Yates, Jr. and W. H. Weinberg which has appeared in *Review of Scientific Instruments* **50**, 132 (1979).]

Preparation and purity measurement of extremely pure helium gas

J. T. Yates, Jr,[a] J. J. Zinck,[b] and W. H. Weinberg[c]

Division of Chemistry and Chemical Engineering, California Institute of Technology, Pasadena, California 91125

(Received 25 September 1978)

A procedure is described for the production, storage, and handling of very pure helium gas and for the measurement of its purity in the part per 10^{11} range.

The preparation and purity measurement of extremely pure He gas is described in this Note. A major contaminant expected in He is H_2, and therefore, our preparation and analytical procedures have focused on the reduction and measurement of H_2 impurity levels. These same procedures are expected to be effective for removal of other chemically active gases.

The ultrahigh vacuum apparatus shown in Fig. 1 has been constructed almost entirely of Pyrex to avoid H_2 outgassing from metal surfaces. It is completely bakeable at 600 K and reaches a base pressure of 1×10^{-10} Torr as measured with a Bayard–Alpert gauge. The pumping speed is approximately 2 l/s. The mass spectrum of residual gases within the apparatus indicates that H_2, CH_4, CO, Ar, and CO_2 are the major impurities present. A 0.3 cm^2 area Rh(111) crystal is supported on Ta heating wires in the apparatus. H_2 adsorption on this crystal can be measured using thermal desorption mass spectrometry; hence, the crystal is an integrating detector for contaminants. Purified helium is prepared by effusion through a heated Vycor leak with storage behind valve V_4.

Following bakeout and achievement of the limiting pressure, the two Ti film getters are activated by evaporation of Ti from W loops containing cross-welded Ti wire sections. The geometrical area of the Ti getter films is 300 cm^2. The Vycor leak is then outgassed at 1025 K until its outgassing cannot be detected using the Bayard–Alpert gauge in the 10^{-10} Torr region. Valve V_4 is then closed and He is effused through the Vycor leak at 975 K. The He used on the high pressure side is specified to be 99.9999% pure as supplied in its cylinder and it is admitted at approximately 1 atm pressure to the high pressure side of the Vycor leak, which is initially between 10^{-7} and 10^{-8} Torr. Typical effusion rates are approximately 6×10^{14} He atoms s^{-1} at 975 K. Storage of the He takes place overnight at several Torr pressure over the freshly evaporated Ti getter film, G_1.

ULTRAHIGH VACUUM APPARATUS FOR PRODUCTION AND PURITY MEASUREMENT OF He

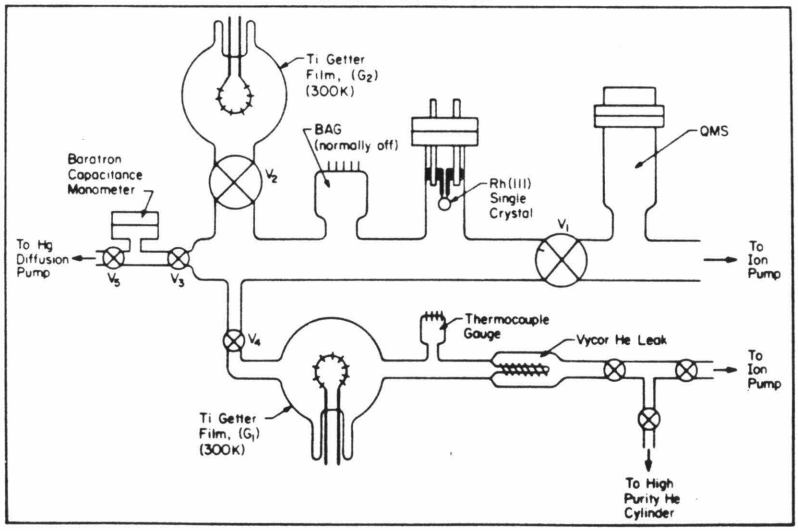

FIG. 1. Ultrahigh vacuum apparatus for production and purity measurement of helium. V_1, V_3, and V_4 are stainless-steel valves. V_2 is a magnetically operated sliding glass valve. BAG—Bayard-Alpert gauge; QMS—quadrupole mass spectrometer.

 0034-6748/79/010132-02$00.60

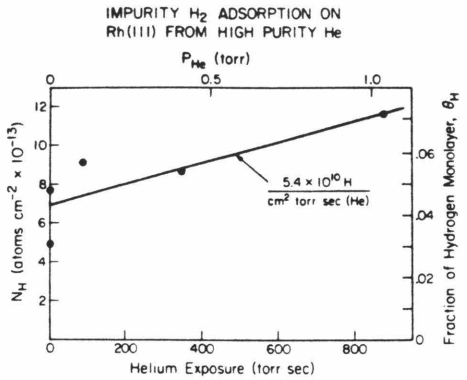

FIG. 2. Impurity hydrogen adsorption on Rh(111) from high-purity He. The rate of adsorption of H_2 from He is calculated assuming that saturation coverage of hydrogen on Rh(111) is 1.6×10^{15} atoms cm^{-2}.

The Rh(111) crystal is cleaned by heating in O_2 to 1050 K and then flashing in vacuum to 1260 K.[1] It may be cooled to 240 K for adsorption of H_2 from the purified He. All adsorption experiments involve preliminary flashing of the crystal to 580 K to remove impurity adsorbed hydrogen and CO.[2] Immediately following this heating program, the system is isolated from the ion pump by closing V_1, and all further pumping of active gases is carried out by getter G_2. The crystal is cooled for 300 s in the static system, and then He is admitted to a pressure of one Torr or less for an exposure of approximately 1000 s to the crystal with V_2 open to the getter film. The He pressure is measured using the bakeable capacitance manometer which is then isolated by closing valve V_3. Following the He exposure, the system is pumped to below 10^{-4} Torr using the Hg diffusion pump which is then closed off at V_3. Final pumping occurs in approximately 60 s through V_1 using the ion pump. This procedure of removing most of the He prior to the use of the ion pump minimizes regurgitation of active gases by the ion pump and reduces crystal contamination significantly.

Valve V_2 to the getter is closed, and the crystal containing adsorbed hydrogen impurity is then heated at a rate of 7.5 K s^{-1}, and the thermal desorption of H_2 is monitored with the mass spectrometer. Calibration of the sensitivity of the mass spectrometer is carried out in control experiments where H_2 desorption is measured from a fully covered Rh(111) crystal exposed to approximately 3×10^{-2} Torr-s of H_2. A saturation coverage of 1.60×10^{15} H/cm^2 [1 H/Rh on Rh(111)] is assumed.

The results of a series of thermal desorption measurements for H_2 are shown in Fig. 2 for various exposures to purified He. Blank experiments with no He admitted yielded approximately 7×10^{13} H/cm^2 with a 1200 s exposure. Assuming an H_2 sticking coefficient of unity, this corresponds to an effective background H_2 pressure of 2×10^{-11} Torr within the static system. The addition of purified He is associated with small increases in the integrated adsorption of H_2. A least-squares fit of the data gives 5.4×10^{10} H/cm^2-Torr-s (He) for the rate of contamination from the purified He. The CO impurity contamination rate is approximately an order of magnitude lower.

From this measurement of the H_2 adsorption rate, one may estimate the ratio of the pressure of H_2 to the pressure of He at the crystal surface, and hence the purity of the He with respect to H_2 contamination. Thus, for a He exposure of 1 Torr-s, the effective hydrogen pressure, $P_{H_2}{}^*$, caused by H_2 contamination in the He is 1.9×10^{-11} Torr. Thus, $P_{H_2}{}^*/P_{He} = 1.9 \times 10^{-11}$.

The time scale for diffusion of impurity H_2 within the apparatus can be estimated from the mutual diffusion coefficient for H_2/He mixtures at one Torr following Hirschfelder *et al.*,[3] where $\sigma_{12} = \frac{1}{2}(\sigma_1 + \sigma_2)$ is the average molecular diameter in Å, M is the molecular weight, and P is the pressure in atmospheres,

$$D_{12} = 2.628 \times 10^{-3} \frac{[T^3(M_1 + M_2)/2M_1M_2]^{1/2}}{P\sigma_{12}} \quad (1)$$

$$= 1.27 \times 10^3 \text{ cm}^2 \text{ s}^{-1}.$$

For H_2/He at 1 Torr, the characteristic time, τ_{max}, for random-walk diffusion through the apparatus of longest dimension $l_{max} \sim 100$ cm is

$$\tau_{max} \cong l_{max}{}^2/2D \cong 4 \text{ s}.$$

Since the typical exposure time is approximately 1000 s in these measurements, the low H_2 contamination rate may not be attributed to a diffusion controlled process at He pressures of 1 Torr or less.

Previous workers have discussed He purification in ultrahigh vacuum systems using superfluid He leaks[4] or diffusion through Vycor.[5,6] In the case of the superfluid He, purity was not measured. For Vycor diffusion without storage over a getter film, a He purity of 10^{-5} H_2/He was estimated using a mass spectrometer. Our procedure makes it possible to improve the Vycor diffusion method by a factor of 10^6, mainly through attention to initial He purity before diffusion and by He storage over a Ti film to remove any diffused H_2 impurity. It is known that H_2 diffusion occurs at about one-tenth the rate of He diffusion through Vycor[4] so that high initial purity coupled with efficient gettering and special vacuum techniques are essential to the production of extremely pure He.

This work was supported by the Dept. of Energy, Division of Physical Research.

[a] Sherman Fairchild Distinguished Scholar. Permanent address: National Bureau of Standards, Washington, DC 20234.
[b] National Research Council of Canada Predoctoral Fellow.
[c] Alfred P. Sloan Foundation Fellow, and Camille and Henry Dreyfus Foundation Teacher-Scholar.

[1] J. T. Yates, Jr., P. A. Thiel, and W. H. Weinberg, Surf. Sci. (in press).
[2] J. T. Yates, Jr., P. A. Thiel, and W. H. Weinberg, Surface Sci., (in press).
[3] J. O. Hirschfelder, C. F. Curtiss, and R. B. Bird, *Molecular Theory of Gases and Liquids* (Wiley, New York, 1954).
[4] M. A Biondi, Rev. Sci. Instrum. **22**, 535 (1951).
[5] F. J. Norton, J. Appl. Phys. **28**, 34 (1957).
[6] J. R. Young and N. R. Whetten, *Transactions of 8th Vacuum Symposium and 2nd International Congress*, American Vacuum Society, 1961, p. 625.